https://doi.org/10.5194/tc-2020-25
Preprint. Discussion started: 3 February 2020

The Cryosphere Discussions

Revealing the former bed of Thwaites Glacier using sea-floor bathymetry

Kelly A. Hogan[1], Robert D. Larter[1], Alastair G. C. Graham[2], Robert Arthern[1], James D. Kirkham[1,3], Rebecca L. Totten[4], Tom A. Jordan[1], Rachel Clark[5], Victoria Fiztgerald[4], John B. Anderson[6], Claus-Dieter Hillenbrand[1], Frank O. Nitsche[7], Lauren Simkins[8], James A. Smith[1], Karsten Gohl[9], Jan Erik Arndt[9], Jongkuk Hong[10], Julia Wellner[5]

[1] British Antarctic Survey, Natural Environment Research Council, High Cross, Madingley Road, Cambridge, CB3 0ET, UK
[2] College of Marine Science, University of South Florida, Saint Petersburg, FL 33701, USA
[3] Scott Polar Research Institute, University of Cambridge, Lensfield Road, Cambridge, CB2 1ER, UK
[4] Department of Geological Sciences, University of Alabama, Tuscaloosa, AL 35487, USA
[5] Department of Earth and Atmospheric Sciences, University of Houston, Houston, TX 77204, USA
[6] Department of Earth Science, Rice University, Houston, TX 77005, USA
[7] Lamont-Doherty Earth Observatory, Columbia University, Palisades, New York, USA
[8] Department of Environmental Sciences, University of Virginia, Charlottesville, VA 22904, USA
[9] Alfred Wegener Institute Helmholtz-Centre for Polar and Marine Research, 27568 Bremerhaven, Germany
[10] Korea Polar Research Institute (KOPRI), Incheon 21990, Republic of Korea

Correspondence to: Kelly A. Hogan (kelgan@bas.ac.uk)

Abstract. The geometry of the sea floor beyond Thwaites Glacier (TG) is a major control on the routing of warm ocean waters towards the ice stream's grounding zone, which has led to increased mass loss through sub-ice-shelf melting and resulting accelerated ice flow. Nearshore topographic highs act as pinning points for the Thwaites Ice Shelf and potentially provide barriers to warm water incursions. To date, few vessels have been able to access this area due to persistent sea-ice and iceberg cover. This critical data gap was addressed in 2019 during the first cruise of the *International Thwaites Glacier Collaboration* (*ITGC*) project, with more than 2000 km^2 of new multibeam echo-sounder data (MBES) were acquired offshore TG. Here, these data along with legacy MBES datasets are compiled to produce a set of standalone bathymetric grids for the inner Amundsen Sea shelf beyond both Pine Island and Thwaites glaciers. At TG, the bathymetry is dominated by a >1200 m deep, structurally-controlled trough and discontinuous ridge, on which the Eastern Ice Shelf is pinned. The geometry and composition of the ridge varies spatially with some parts having distinctive flat-topped morphologies produced as their tops were planed-off by erosion at the base of the seaward-moving Thwaites Ice Shelf, suggesting a positive feedback mechanism for ice-shelf ungrounding. Knowing that this offshore area is a former bed for TG, we applied a novel spectral approach to investigate bed roughness and find that derived power spectra can be approximated using an inverse-square law, a result that is consistent with spectra for bed profiles from the modern TG. Using existing ice-flow theory, we also make a first assessment of the form drag (basal drag contribution) for ice flow over this topography. Ice flowing over the sea-floor troughs and ridges would have been affected by similarly high basal drag to that acting in the grounding zone today. We show that the sea-floor bathymetry is an analogue for extant bed areas of TG and that more can be gleaned from these 3D bathymetric datasets

https://doi.org/10.5194/tc-2020-25
Preprint. Discussion started: 3 February 2020

regarding the likely spatial variability of bed roughness and bed composition types underneath TG. Comparisons with existing regional bathymetric compilations for the area show that high-frequency (finer than 5 km) bathymetric variability beyond Antarctic ice shelves can only be resolved by observations such as MBES and that without these data calculations of the capacity of bathymetric troughs, and thus oceanic heat flux, may be significantly underestimated. This work meets the requirements of recent numerical ice-sheet and ocean modelling studies that have recognised the need for accurate and high-resolution bathymetry to determine warm water routing to the grounding zone and, ultimately, for predicting glacier retreat behaviour.

1 Introduction

Knowledge of Antarctica's coastal bathymetry is essential when considering ocean circulation and recent dynamic changes at the ice-sheet margin. Sea-floor bathymetry influences ice-ocean interactions in two ways. First, deep (> 500 m water depth) bathymetric troughs and channels provide access routes for warm, salty Circumpolar Deep Water (CDW: ~ 0.5-1.5 °C, located below ~300-500 m water depth; Jacobs et al., 1996, 2013) to present-day grounding zones. The inflow of CDW increases basal melting and ice-shelf thinning (Jacobs et al., 1996; Rignot et al., 2013) leading to grounding-zone retreat, reduced ice-shelf buttressing and ultimately the acceleration of the ice shelves and grounded ice upstream (Schoof, 2007; Joughin et al., 2010; Favier et al., 2014; De Rydt & Gudmundsson, 2016). This effect is particularly significant for ice resting on reverse-slope beds (i.e. retrograde, when the bed slopes down towards the interior of the continent) where grounding-zone retreat may initiate marine ice sheet instability, a positive feedback that could lead to runaway retreat (Weertman, 1974; Schoof, 2007). Secondly, bathymetric highs can slow ice retreat by acting either as pinning points for floating ice or as "sticky spots" at the grounding zone itself, and by partially blocking warm water access to modern grounding zones (e.g. De Rydt et al., 2014). An ice shelf pinned on a bathymetric high is subject to increased buttressing, and a topographic high at the grounding zone similarly contributes to basal drag that restricts ice flow. Both have the potential to act as stabilising influences (Alley et al., 2007; Parizek & Walker, 2010).

Obtaining direct sea-floor measurements at marine-terminating ice-sheet margins is often difficult due to more or less persistent floating ice cover in the form of icebergs, ice tongues, ice shelves and sea ice. This is certainly the case at Thwaites Glacier (TG), West Antarctica, which is one of the two dominant fast-flowing glaciers draining into the eastern Amundsen Sea Embayment (ASE) (Fig. 1); the other being Pine Island Glacier. Together, Thwaites and Pine Island glaciers were responsible for >30 % of the annual ice discharge from the West Antarctic Ice Sheet (WAIS) between 2009 and 2017 (compared with 25 % for 1979-1989; Rignot et al., 2019), and TG alone accounted for ca. 55% of the annual mass balance from the WAIS between 1992 and 2017 (Shepherd et al., 2019). Recent observations and mass balance calculations show that TG is experiencing some of the highest rates of flow acceleration (Mouginot et al., 2014), discharge (Rignot et al., 2019), thinning (McMillan et al., 2014; Milillo et al., 2019; Shepherd et al., 2019), and grounding-line retreat (Rignot et al., 2014; Milillo et al., 2019) across the entire ice sheet. For example, over the past three decades net mass loss from TG is calculated to have increased from 12±1

https://doi.org/10.5194/tc-2020-25
Preprint. Discussion started: 3 February 2020

Gt yr^{-1} during the period 1992-1997 to 76±6 Gt yr^{-1} from 2012 to 2016 (Shepherd et al., 2019). Its configuration, on a reverse-bed slope with direct connectivity to the deep WAIS interior (Holt et al., 2006) and its wide marine-terminating ice front (>120 km) with only small, unconfined frontal ice shelves, implies that TG is particularly susceptible to retreat via marine ice sheet instability (Weertman, 1974; Hughes, 1981; Vaughan & Arthern, 2007; Schoof, 2012). Furthermore, a significant retreat in this system could lead to a much wider WAIS collapse and the future behaviour of this glacier system is now in the spotlight (e.g. Joughin et al., 2014; Scambos et al., 2017).

At present, the eastern and central parts of TG are fronted by two protruding floating ice masses, the Eastern Ice Shelf (EIS) and the Thwaites Glacier Tongue (TGT), which extend for 40-50 km beyond the grounding zone, to the west of which a 20-km wide mélange of icebergs and sea-ice exists (Fig. 2). For simplicity, we shall refer to these floating ice masses collectively as the Thwaites Ice Shelf (Fig. 2a; cf. Heywood et al., 2016). The TGT extends from the fastest-flowing region of TG (Fig. 2a) and has periodically advanced to extend up to 130 km from the grounding line before the majority of the floating tongue has calved (MacGregor et al., 2012). As a result, the inner shelf beyond this area has been rendered inaccessible by remnants of the TGT as they have drifted north-northwest, including the very large B-10 and B-22A icebergs that remained grounded on the shelf for decades after they had calved before 1972 and in 2002, respectively (Fig. 1) (Ferrigno et al., 1993; Rabus et al., 2003; MacGregor et al., 2012). In contrast, the EIS remains pinned on a sea-floor high that restricts its flow (Rignot et al., 2001; Tinto and Bell, 2011; Jordan et al., 2020) and induces shear between the EIS and TGT. Satellite imagery confirms that since 2006 increased crevassing and fracturing has weakened the shear zone between the EIS and TGT (Kim et al., 2015), with the two ice shelves remaining connected until 2010 (MacGregor et al., 2012). Due to its inaccessibility, few marine observations have been made on the inner shelf in front of TG (Jacobs et al., 2012). The existing hydrographic data, along with more comprehensive results from Pine Island Bay, confirm the presence of CDW in the deep troughs east and north of the EIS (Dutrieux et al., 2014; Jenkins et al., 2016) and identify these troughs as potential pathways for warm water to the TG grounding zone (Fig. 2a; Milillo et al., 2019).

Regional bathymetric compilations for the ASE shelf use multibeam echo-sounder data (MBES) where available in offshore regions (Nitsche et al., 2007, 2013; Arndt et al., 2013) and gravity inversions and a limited amount of echo-sounding data from autonomous underwater vehicles for sub-ice shelf cavities (Jenkins et al., 2010; Tinto and Bell, 2011; Millan et al., 2017; Jordan et al., 2020.). These datasets have identified glacially-modified depressions on the continental shelf that act as conduits for CDW transport towards present-day ocean-terminating glacier margins in the ASE (Fig. 1) (e.g. Nitsche et al., 2007; Walker et al., 2007; Jacobs et al., 2012; Nakayama et al., 2013). Landward of the MBES data coverage that existed prior to this study, gravity inversions had indicated the presence of an east-west trending ridge on which the EIS is pinned (Rignot, 2001; Tinto & Bell, 2011; Millan et al., 2017). Millan et al. (2017) reported that the ridge is interrupted by at least three channels with water depths between 600 and 1000 m, interpreted to be potential CDW pathways towards the grounding zone.

Here, we present the first direct observations of sea-floor bathymetry adjacent to Thwaites Ice Shelf acquired as part of the first *International Thwaites Glacier Collaboration* (*ITGC*) cruise on RV/IB *Nathaniel B. Palmer* in January–March 2019 (cruise NBP19-02). In the first part of the paper, we use these data to investigate the character (bed geometry and substrate

https://doi.org/10.5194/tc-2020-25
Preprint. Discussion started: 3 February 2020

composition) of topographic highs as former grounding zones and ice-shelf pinning points, and to better resolve sea-floor troughs as potential modified CDW (CDW) pathways to the modern Thwaites grounding zone. In the second part of the paper, we use a spectral approach to relate flow-line roughness to the drag contribution for an overriding ice mass using bathymetric profiles from the inner ASE shelf, and bed profiles from upstream areas of Pine Island and Thwaites glaciers. To reflect these two components, (1) we describe the observational (geophysical) datasets used and interpret the new bathymetric dataset, which is also provided as a publically-available standalone grid and (2) we describe the spectral approach and use it to quantitatively examine former and modern TG beds. We demonstrate that the offshore area just seaward of Thwaites Ice Shelf is an appropriate analogue for the modern grounding zone of TG, both in terms of its bed characteristics and in the effect of its rugged bed topography on ice flow by calculating drag contribution for different scales of roughness. We highlight the importance of high-resolution MBES observational data for constraining gravity inversions and regional bathymetry compilations, which are essential boundary conditions for predictive numerical modelling experiments, and for accurately calculating the flux of warm water to the grounding zone.

2 Geophysical datasets

2.1 Multibeam echosounder datasets (MBES)

During *ITGC* cruise NBP19-02, the marine areas in front of TG were unusually clear of sea-ice and icebergs providing a unique opportunity for bathymetric data acquisition at the margin of Thwaites Ice Shelf (Larter et al., 2020). MBES data was acquired using a hull-mounted 1° x 1° Kongsberg EM122 echo sounder with 288 across-track beams and an operational frequency in the range 11.25-12.75 kHz. The MBES was configured with "High Density Equidistant" beam spacing meaning that more than one sounding can be produced per beam (up to 432) effectively increasing across-track resolution, and in "Dual Ping" mode which ensures equal across- and along-track sounding spacing. As an example, in 600 m water depth with a 60° beam angle (typical conditions and settings on NBP19-02), this results in a sounding spacing on the sea floor of ~5-7 m. Here, in addition to this new dataset, we have compiled all available MBES data in the area from UK, US, German, Swedish and Korean expeditions (Table 1; Fig. 2) to produce gridded bathymetric data products.

For NBP19-02, data processing was performed on board using MB-System (Caress and Chayes, 1996; Caress et al., 2019) in order to apply optimal sound velocity profiles (SVPs) to each data file and to remove erroneous soundings. Ray tracing and sea-floor depths were calculated using SVPs generated from conductivity-temperature-depth and expendable bathythermograph casts made during NBP19-02 (Larter et al., 2020). Most of the other bathymetry datasets were also initially ping-edited during each respective cruise; however, minor additional cleaning was performed in MB-System and QPS Fledermaus (Mayer et al., 2000) after the datasets were collated when clear outliers could be easily identified. Ultimately, the data were gridded in MB-System using a Gaussian weighted mean filter algorithm to produce an isometric 50-m digital elevation model (DEM) for the sea floor on the southern ASE shelf. A degree of interpolation was applied to the final grids in data gaps only, filling areas six cell widths away from cells with real soundings, i.e. for a 50-m grid interpolation will fill cells

https://doi.org/10.5194/tc-2020-25
Preprint. Discussion started: 3 February 2020

up to 300 m away from a cell with real soundings. A lower resolution DEM (500-m grid cells) was produced for studies that typically use coarser bathymetric information. Together, the 50-m and 500-m DEMs are presented as a standalone regional mid-resolution bathymetric dataset. In addition, in order to examine the nature of specific sea-floor features (e.g. ice-shelf pinning points), higher-resolution grids (30-m grid cells) were produced where sounding densities allowed (e.g. Fig. 4). Final grids were visualised and analysed in QPS Fledermaus and ArcGIS 10.6. Sea-floor trough and channel metrics (including widths, depths, symmetry, form ratio, u-/v-shape characterisation) were derived using the methods described in Kirkham et al. (2019).

2.2 Bed profiles for investigating bed roughness and basal drag

The gridded bathymetric datasets that we have produced represent the former bed of an expanded TG. Palaeo-flow lines across this former bed were picked manually by tracing lines parallel to subglacial landforms taken to indicate palaeo-ice flow directions (e.g. Fig. 3b). We also perform this exercise for bed profiles from three additional areas for comparison with the Thwaites offshore area (Figs. S1, S2): (i) modern along-flow bed profiles for Thwaites Glacier and (ii) Pine Island Glacier, and (iii) an area of "smooth" bed topography on the middle continental shelf in the Dotson-Getz palaeo-ice stream trough, offshore from the Getz A Ice Shelf, representing a sedimentary palaeo-ice stream bed characterised by mega-scale glacial lineations (MSGL) (Graham et al., 2009; Spagnolo et al., 2014). Onshore bed profiles were extracted from the AGASEA (Holt et al., 2006) and Operation IceBridge (Cochran & Bell, 2010, updated 2014) datasets for Thwaites and Pine Island glacier beds, respectively; the profile from the Dotson-Getz Trough was extracted from an MBES dataset fully described by Larter et al. (2009) and Graham et al. (2009).

3 New bathymetric compilation for the inner Amundsen Sea Embayment shelf

Our bathymetric compilation includes more than 2000 km^2 of new MBES data between the EIS and the TGT and west of the TGT that provides near-continuous bathymetric coverage for ~40 km north of the present day ice-shelf margin (Figs. 2, 3). Data gaps remain in the western part of the area in front of the ice mélange, east of Crosson Ice Shelf, as icebergs and bergy bits released from the ice mélange persistently covered this region during NBP19-02. In addition, perennial fast ice and huge icebergs, such as the 80-km long and 45-km wide iceberg B-22A, that calved periodically from the TGT and then moved slowly north- and northwest, thereby episodically running aground, have generally prevented survey between TGT and Crosson Ice Shelf (see area with B-22A outlines on Fig. 1).

The sea-floor bathymetry offshore Thwaites Ice Shelf is dominated by an elongate depression oriented NNE-SSW (T1) and a series of topographic highs (H1-H3) along its southern margin (Fig. 3a). The depression is characterized by water depths of 1100-1250 m, which is 200 to 400 m deeper than the sea floor on its flanks; it typically has a relatively flat or gently-inclined floor (Figs. 3a, c). Although the depression appears to be continuous for at least 75 km, and connects with areas of deep (>1300 m) sea floor directly north of the EIS and in Pine Island Trough further east (Fig. 2a), its width varies significantly along its

https://doi.org/10.5194/tc-2020-25
Preprint. Discussion started: 3 February 2020

length and the flanks are discontinuous in form. As a result, we do not define this feature as a "channel", which implies incision by water flow, but rather as a small trough. The topographic highs that make up the southern flank of the trough (H1-H3) decrease in height (above the surrounding sea floor) from east to west and appear to form a broad (>15 km) but discontinuous ridge, also oriented NNE-SSW. The large, discontinuous ridge is the extension of a bedrock ridge in Pine Island Trough to the east that has the same orientation (Figs. 2, 3a; Nitsche et al., 2013). The most prominent high (H1) occurs immediately north of the EIS with a shallowest recorded water depth of just 82 m and extends at least 40 km in a north-south direction. The northern part of the EIS is pinned, about 45 km downstream of the grounding zone (Rignot et al., 2001; Tinto and Bell, 2011; MacGregor et al., 2012), on the southern part of this high, forming an ice rumple in the EIS (Matsuoka et al., 2015). The shallowest water depths on the two highs H2 and H3 (from NNE to SSW) are 362 m and 611 m, respectively. Indeed, remote-sensing data had identified a pinning point for TGT on H2 (Rignot et al., 2011) but the TGT must have fully retreated from that point prior to NBP19-02. North of the trough and ridge (north of 74°30' S) is an area of rugged morphology characterised by shallow sea floor ridges and deep basins (>1400 m); this area merges with similar terrain in Pine Island Trough described by Nitsche et al. (2013) as their "area 2" (Fig. 2). East of the EIS, the eastern flank of H1 is just exposed but the bathymetry is dominated by a deep (1000-1200 m), rugged area of sea floor, bounded on its eastern edge by a bedrock high in Pine Island Bay that continues southward towards the grounding line (Fig. 2a). The deepest part of this area appears to form a poorly-defined bathymetric trough oriented NNE-SSW (T4; Fig. 3a); oceanographic measurements and models confirm that this deep acts as a pathway for CDW towards grounding lines in western Pine Island Bay (Fig. 2a) (Dutrieux et al., 2014; Nakayama et al., 2019).

3.1 Glacial landforms

The large-scale morphology of the sea floor offshore Thwaites Ice Shelf is overprinted by linear features oriented sub-parallel to the trough and ridge. Streamlined subglacial landforms occur in areas where bedrock crops out at the sea floor, on either topographic highs or interrupting the smooth trough floor or rugged basin floors (Figs. 3a, b). These features are identified as crag-and-tails by their tapering form and are 750-4000 m long, 200-2000 m wide and 25-250 m high (Figs. 3, 4), and their morphological similarity to crag-and-tails from other deglaciated terrains (e.g. Dowdeswell et al., 2016; Maclean et al., 2016; Nitsche et al., 2016). The wider southern ends of the crag-and-tails are rugged and have significant relief, suggesting bedrock composition, whereas the northern ends are smooth and elongate, suggesting sedimentary composition. These landforms are produced subglacially as glacier ice flows across bedrock obstacles producing the characteristic morphology through erosion and deposition (Benn & Evans, 2010; Nitsche et al., 2016). The tapering of these features north-northeastward indicates palaeo-ice flow of TG in this direction towards Pine Island Trough (Fig. 3b); east of the EIS the orientation of these landforms varies from N-S to NW-SE depicting flow around the H1 high (Fig. 3b). Curved or semi-circular moats - crescentic scours (Lowe and Anderson, 2003; Graham et al., 2009; Graham and Hogan, 2016) - occur around the southern (upstream) sides of some crag-and-tails (Figs. 3, 4) and are suggestive of erosion by meltwater (or a till slurry) upstream of bedrock obstacles (cf. Graham & Hogan, 2016). On the H2 and H3 highs, subtle elongate ridges separated by linear grooves also occur. These glacial

https://doi.org/10.5194/tc-2020-25
Preprint. Discussion started: 3 February 2020

lineations have parallel sides, lack a pronounced and wider end, and are 1000-2500 m long, 100-200 m wide and 2-10 m high. These features, which were produced subglacially, have relatively short elongation ratios (<10:1) and are oriented parallel to crag-and-tails also on the tops of the highs but are slightly oblique to crag-and-tails in the trough (Fig. 3). A distinct but discontinuous scarp is mapped on the top of the H2 high, upstream from its frontal edge (Figs. 3, 4b, 4d). The scarp has a curved planform and a steep (3-4°) northern and gentle (0.5°) southern slope; glacial lineations occur on the gentle back-slope of this feature which extends for about 15 km in a SW-NE direction. The asymmetric geometry and lineated back-slope of this landform identify it as a grounding-zone wedge (GZW) (Alley et al., 1989; Larter and Vanneste, 1995; Dowdeswell & Fugelli 2012; Jakobsson et al., 2012), i.e. a wedge of sedimentary material that built up at the grounding line when it was stable for a time on the H2 high. This feature is interrupted, however, by a ~40 m deep groove or small channel with bedrock ridges visible on either side suggesting that the sedimentary wedge is not thick enough to fully bury the underlying topography, i.e. it is only tens of metres thick. Discrete 6-10 m deep linear to curvilinear furrow with small berms (4-6 m) were mapped and on H3 and north of the GZW front scarp (Figs. 4a, b); these are interpreted as iceberg ploughmarks.

Sea-floor highs in the area are also variously gouged and streamlined, resulting in a pattern of grooves and bedrock ridges. Grooves on the H1-H3 ridges occur on their southern (upstream) parts and exhibit a range of orientations that probably relate to the structure of the underlying bedrock exploited by glacial erosion. The grooves are typically <20 m deep, <200 m wide and <6000 m long. The surfaces of sea-floor highs north of the H1-H3 ridge have a more streamlined appearance resulting from shallow, semi-parallel shallow grooves that are preferentially aligned with the crag-and-tails (Figs. 2, 3). This type of streamlined bedrock highs is typical of inner-shelf morphologies around Antarctica (e.g. Wellner et al., 2006; Livingstone et al., 2013) including in the adjacent eastern part of Pine Island Bay (Nitsche et al., 2013). Taken together, the orientations of the streamlined glacial landforms (crag-and-tails, glacial lineations, bedrock grooves/ridges) define the former ice-flow directions of an expanded TG (depicted by red arrows in Fig. 3b).

3.2 Trough and channel metrics

Multiple bathymetric troughs and bedrock channels were mapped and analysed in the area beyond Thwaites Ice Shelf as part of this study (Fig. 3a). Troughs and channels in the adjacent eastern part of Pine Island Bay have been described comprehensively by Nitsche et al. (2013) and Kirkham et al. (2019). The larger troughs in our study area, which have also been identified on gravity-derived regional bathymetry maps (Millan et al., 2017; Jordan et al., 2020.), are considered important as potential pathways for the transport of CDW towards the grounding zone of TG and warrant full description here. We distinguish these comparatively larger troughs, based on their size, connectivity and variable flank form (as described above), from the channels which are notably smaller in scale (Fig. S3) with continuous, parallel sided-flanks, undulating thalwegs, and incise into rugged sea-floor areas interpreted as bedrock. It is widely accepted that channels of the latter type were eroded by pressurised subglacial water flow (Lowe and Anderson, 2003; Nitsche et al., 2013; Kirkham et al., 2019), whereas the troughs likely relate, at least in part, to underlying geological structures such as mafic dykes and tectonic deformations (cf. Gohl et al., 2013) that have been variously modified by ice.

https://doi.org/10.5194/tc-2020-25
Preprint. Discussion started: 3 February 2020

Cross-sectional analyses of the troughs reveal their large scale, with average widths, depths and cross-sectional areas being 2090 m, 90 m and 144 000 m^2, respectively (Fig. S3). The troughs are typically 10-30 times as wide as they are deep, although we note that there is a significant size difference between the main NE-SW trough (T1) and the remaining troughs (Fig. 3a; Fig. S3). By comparison, the bedrock channels are on average 520 m wide, 50 m deep with a cross-sectional area of 18 000 m^2. The channels are generally 5-10 times wider than they are deep. The derived *b values*, which characterise cross-sectional shape (Pattyn and Van Huele, 1998), suggest that the bedrock channels are between v- and u-shaped, whereas the larger troughs have no dominant cross-section shape (Fig. S3). In general, the trough floors are flat or inclined in cross-profiles (Fig. 3c), and are gently undulating in along-trough profiles.

The main T1 trough is oriented NNE-SSW, which is oblique to the northerly palaeo ice-flow directions immediately in front of Thwaites Ice Shelf (Fig. 3b). This indicates that, at the time that the subglacial landforms were produced, ice was thick enough not to be steered by even major elements of the bed topography. The two southernmost troughs (T2 and T3 on Fig. 3a) are oriented perpendicular to TI (i.e. NNW-SSE), and the troughs north and east of the EIS are generally aligned with palaeo-ice flow directions (Figs. 2, 3a). The T2 and T3 troughs, whose floors have water depths of 800-900 m, separate the H1-H3 bathymetric highs and are of interest as potential pathways for CDW to the TG grounding line.

3.3 Bathymetric highs and ridges

Owing to the importance of sea-floor highs in front of the Thwaites Ice Shelf as barriers to CDW inflow, and as former ice shelf/sheet pinning points, we examine the morphology of the discontinuous NNE-SSW trending ridge in detail (Fig. 4). The ridge comprises the H1-H3 highs separated by the two troughs described above (T2 and T3; Fig. 3a). The width of the ridge varies significantly, from 6 km in the SW of the study area to at least 40 km over H1, although we acknowledge that data coverage is limited. In places, the bathymetric highs are strikingly flat-topped. These planar features are accentuated in maps of the first derivative of bathymetry, slope, which reveals both low slopes (<2°) (Figs. 4c, d), and low roughness over H2, H3 and the western part of H1. The continuation of the ridge further north into Pine Island Trough has a similar surface expression but is generally narrower (Fig. 3a). These areas with low surface slopes are atypical when compared with other bathymetric highs in the area, which have rugged surface morphologies characterised by bedrock grooves and channels (Fig. 2, 4d) (Nitsche et al., 2013; Arndt et al., 2018; Kirkham et al., 2019). Instead, the low slope values are similar to those derived for the base of the troughs in front of Thwaites Ice Shelf (Fig. 4a) and the sediment-filled basins just seaward of the Pine Island Ice Shelf front (Nitsche et al., 2013; Kuhn et al., 2017). At least three distinct levels of flat-topped surfaces occur at 400 m, 570 m and 620 m water depth (Fig. 5). We interpret this morphology as being generated during a prolonged period of overriding by a formerly expanded Thwaites Ice Shelf (with the necessary ice thickness). Support for this comes from the orientation of glacial lineations on the tops of the highs (Fig. 3b), which are in line with modern ice-velocity vectors (Mouginot et al., 2019) but oblique to the orientation of crag-and-tails in the troughs. A similar interpretation was made for the lineated surface of a former pinning point of the Pine Island Ice Shelf (PIIS) that has been recently exposed by ice-shelf calving events (Arndt et al., 2018), although that feature was not planed off to form a flat-topped high but rather has a stepped and rugged surface morphology

https://doi.org/10.5194/tc-2020-25
Preprint. Discussion started: 3 February 2020

albeit with some gently-sloping parts (see their Fig. S3). The morphology of the highs in our study area is striking and notably rare for sea-floor highs around Antarctica. However, we do identify a similar but less pronounced terrain over some highs along the same structural ridge in eastern Pine Island Bay, i.e. east of the EIS (Fig. 5b), and a solitary planed-off high, with comparable dimensions to those offshore TG, is visible <5 km north of the Getz-A Ice Shelf (Fig. 5c). Outwith these rare examples, the best analogy for this morphology probably comes from a set of "iceberg terraces" on terminal moraines at the mouth of a Svalbard fjord, which display remarkably flat-topped surfaces at several bathymetric levels. These are interpreted to have formed as tabular, flat-based icebergs over-topped and eroded morainal sediments (Noormets et al., 2016). It should be noted, however, that sediments of this morainal bank complex probably consist of unconsolidated material that has not been overridden (or compacted) by grounded ice, meaning that they are likely more erodible than the basement highs in front of Thwaites Ice Shelf.

New geomorphic information is also revealed by the flanks of the highs (Figs. 4a, b). The northern (ice distal) flank of the H2 and H3 highs are characterised by subtle down-slope trending gullies that transition into a smooth but inclined sea floor in the troughs at a distinct break of slope. In addition, there are a few, discrete semi-circular indentations in the scarp between the surface of the highs and their flanks (Fig. 4a). The gullies have simple non-branching geometries, small dimensions (widths 150-700 m, depths 5-50 m, lengths <2 km), and typically define broad u-shapes in cross-section, although some v-shaped forms are present. In addition, their long-profiles have negative slopes (i.e., deepen consistently down the flank of the highs) and their form is consistent with other Antarctic submarine gully systems (e.g. Gales et al., 2013; Post et al, 2019). Thus, we interpret the gullies as the result of the down-slope mass movement of material from the tops and sides of the H2 and H3 highs via gravitational processes into the small sediment fans at the base of the slope (Fig. 4a). The semi-circular indentations may be the headwalls of small slide scars (cf. Noormets et al., 2009; Gales et al., 2013). One 6 km by 2.6 km segment of the H3 high is somewhat detached from other parts of the ridge and appears particularly fragmented on its flanks (Fig. 4a). About 1500 m south of this, on the main H3 high, is a distinct break in slope with the same planform shape as the back of the detached segment that we refer to as a "block" (bl in Figs. 4a, c). Similarly, 2 km west of this block is another somewhat isolated 3 km by 1.8 km block of H3 that is incised by gullies on its northern front and lacks lineations on its surface (Fig. 4a). We consider several interpretations for these features: First, it is possible that they are detached slide blocks of the H3 high that had been displaced down-slope over a short distance (black arrows in Figs. 4a, c), remaining largely intact, but subsequently affected by some gravitational collapse of their flanks. Slide "megablocks" with similar dimensions (or larger), non-crystalline compositions, and degraded flanks are known from, for example, the Hinlopen Slide scar on the northern Barents Sea margin (Vanneste et al., 2006; Hogan et al., 2013). The second possibility is that the blocks are small bedrock highs that have been variously mantled by and surrounded by glacigenic sediment as it was transported down-slope (towards the sediment fans) from the H3 high (see blue arrows on Fig. 4a). If the latter case is true, then the pronounced semi-circular indentation on the eastern block (labelled in Fig. 4a) may be an erosional scour mark formed by persistent bottom water motion, as is evidenced by the small channel on the eastern side of the block (white arrows in Fig. 4c).

https://doi.org/10.5194/tc-2020-25
Preprint. Discussion started: 3 February 2020


The Cryosphere Discussions

4 Bed roughness and basal drag

4.1 Spectral analysis of bed roughness

The high-resolution bathymetric grid that we have produced (Fig. 2) represents the former beds of expanded Thwaites and Pine Island glaciers. As such, it contains information about bed geometry and roughness that can be used to investigate the behaviour of glacier ice over this terrain, specifically how roughness at the bed (e.g. bedrock topography and subglacial landforms) might generate "form drag" (Schoof, 2002) within the ice. The bathymetry contains roughness at various wavelengths, λ, each equivalent to a spatial frequency f=1/λ. We use power spectra of the high-resolution bathymetry (Figs. 6, 7), together with a theoretical expression for form drag (Schoof, 2002, equation 67) to recover the drag caused by undulations at each spatial frequency. The theoretical expression applies to flow lines and was applied to palaeo- and modern flow lines for TG and the Dotson-Getz palaeo-ice stream as described in Section 2.2 (locations in Fig. S1).

To analyse the variance of roughness at each wavelength scale we computed the power spectrum of the bathymetric topography (Figs. 6, 7). As an example, Figure 6a shows a bed elevation profile (location in Fig. S1) sampled at 25-m intervals along a flow line. Figure 6b shows the derived one-sided periodogram $P(f_n)$, evaluated at a set of equally-spaced spatial frequencies $f_n = \lambda_n^{-1} = n/a$, where a is the length of a moving window. The periodogram was obtained using Welch's method (Welch, 1967), with a Hamming window of length a =6.4 km and 50% overlap between consecutive windows along the bed profile. The periodogram shows no strong peaks at any particular preferred scales of roughness (Fig. 6b). Instead, the variance of roughness decreases continuously as spatial frequency increases and the reduction of variance with increasing spatial frequency approximately follows an inverse-square power law so that the periodogram can be approximated as $P_n = P(f_n) = Af_n^{-2}$. This is the power spectrum of a fractal 'Brown-noise' or random-walk elevation profile, as would be produced by adding an uncorrelated random offset in the vertical for each unit-length step taken in the horizontal. The inverse-square law provides a good approximation to all power spectra observed (Figs. 7, SF4), so the variance of roughness at any particular frequency scales inversely to the square of that frequency and proportionately to the coefficient, A. The red line in Figure 6b corresponds to a value A = 0.1 m and the spectra are remarkably consistent across many of the profiles considered (Figs. 7, SF4) with the exception of the smoother MSGL area that is discussed in section 4.2.

The power-law approximation to the power spectrum provides reasonable agreement for multiple flow lines from the offshore bathymetry (Figs. 7, SF4). It also agrees closely to power spectra of profiles of bed elevation from airborne radar flown over TG (Fig. 7c), so the MBES data provide an analogue to the subglacial undulations that control the sliding of Thwaites Glacier today. Despite improvements in the methodology of high-resolution radar surveys of the active subglacial bed (King et al., 2016; Bingham et al., 2017), the MBES provides a more detailed view of the shorter spatial scales than airborne or ground-based radar.

https://doi.org/10.5194/tc-2020-25
Preprint. Discussion started: 3 February 2020


The Cryosphere Discussions

4.2 Relating bed topography to basal drag

In this section, we will use a theory of ice flow to assess how the roughness at these different scales will affect the drag that opposes glacier sliding. As demonstrated above, the power-law approximation is appropriate for bed profiles from both the bathymetric data as well as for bed profiles from airborne radar data. This allows us to consider the contribution that the observed sea-floor bathymetric roughness at short wavelengths would make to form drag when covered by flowing ice. The theory of ice flow over an undulating bed (Schoof, 2002) provides an approximate expression for the form drag τ, expressed as a basal shear stress that acts to resist sliding:

$$\tau = \beta U \quad \text{(eqn. 1)}$$

In this expression, U is the speed of ice flow averaged over some horizontal length scale (here, chosen as a, the window length, i.e. the longest wavelength considered in the spectral analysis) and β is the drag coefficient. According to Schoof (2002), the drag coefficient $\beta = \sum_{n=1}^{\infty} \beta_n$ is the sum of contributions β_n , each of which is caused by roughness at a different wavelength scale λ_n. As per the spectral analysis above, these wavelengths correspond to equally-spaced spatial frequencies $f_n = \lambda_n^{-1} = n/a$, and spatial wavenumbers $k_n = 2\pi f_n$.

Schoof (2002) provides an expression for the drag contributed by each spatial frequency:

$$\beta_n = 4\beta^*(k_n/k^*)^3 F(k_n/k^*)\left|\hat{h}_n/H\right|^2 \quad \text{(eqn. 2)}$$

In this expression, $\hat{h}_n$ is the Fourier component of the bed roughness at spatial frequency f_n. The scaling constants are $\beta^* = \eta/H$ and $k^* = 1/H$, where η and H are representative viscosity and thickness, respectively, averaged over the length scale a (Schoof, 2002). We estimate the squared magnitude of the Fourier component of the roughness using the one-sided periodogram, $\left|\hat{h}_n\right|^2 = \frac{1}{2}P_n H^{-2} a^{-1}$. This corresponds to the definition of the roughness Fourier series used by Schoof (2002). We consider two limiting cases for the function F:

$$F_1(k_n/k^*) = \frac{\sinh^2(k_n/k^*) - (k_n/k^*)^2}{(k_n/k^*) + \cosh(k_n/k^*)\sinh(k_n/k^*)} \quad \text{(eqn. 3)}$$

$$F_2(k_n/k^*) = \frac{(k_n/k^*) + \sinh(k_n/k^*)\cosh(k_n/k^*)}{\sinh^2(k_n/k^*)} \quad \text{(eqn. 4)}$$

These are derived by Schoof (2002) (equations 65 and 66 for small and large bed roughnesses, respectively). Note that we have used dimensional quantities throughout, so $k_n/k^*, \hat{h}_n/H$ and $F(k_n/k^*)$ in our notation are equivalent to non-dimensionalised quantities k_n, $v\hat{h}_n$ and $f(k_n)$ respectively in Schoof's notation.

https://doi.org/10.5194/tc-2020-25
Preprint. Discussion started: 3 February 2020


The Cryosphere Discussions
Open Access
EGU

For the same example bed profile in Figure 6a, values of β_n/β^* are plotted against spatial frequency f_n in Figure 6c for a representative ice thickness $H = 1$ km. For sufficiently small features, so that $k_n \gg k^*$, the functions $F_1(k_n/k^*)$ $F_2(k_n/k^*)$ both tend to unity. Then the form drag becomes insensitive to ice thickness and to the choice of function used (Schoof, 2002). In those circumstances, we can use $k_n = 2\pi f_n = 2\pi n/a$, with the inverse-square law $P_n = Af_n^{-2} = Aa^2n^{-2}$, to show that the drag contribution β_n will grow approximately linearly with frequency according to:

$$\beta_n = 16\eta\pi^3 Aa^{-1}f = 16\eta\pi^3 Aa^{-2}n \quad \text{(eqn. 5)}$$

Even though the amplitude of roughness decreases at shorter wavelengths, our results, combined with the theory, show that those short scales will be more effective at causing form drag. This is because the factor $(k_n/k^*)^3$ increases faster than the inverse square law decreases. The resulting linear dependence is shown as a red line on Figure 6c. As a consequence of the linear increase in the drag contribution with frequency, the total drag would become unbounded, and the sliding would stop, unless the bathymetry becomes smooth at scales smaller than some wavelength λ_N. This wavelength provides an upper bound to the spatial frequency $f_N = \lambda_N^{-1} = N/a$. Under this assumption, the total drag can be approximated by:

$$\beta = \sum_{n=1}^{N}\beta_n = 16\eta\pi^3 Aa^{-2}\sum_{n=1}^{N} n = 8\eta\pi^3 Aa^{-2}N(N+1) \quad \text{(eqn. 6)}$$

When $\lambda_N \ll a$, so that $N \gg 1$, this gives the approximation:

$$\beta = 8\eta\pi^3 A\lambda_N^{-2} \quad \text{(eqn. 7)}$$

Therefore, if the observed inverse-square law power spectra applies down to the finest length scale λ_N, the drag will be determined by that scale, along with the viscosity η, and the coefficient of the power law A recovered from the periodograms. It is common in sliding theories to define the slip length, $L = \eta/\beta$. This lets us make a dynamical distinction between regions of fast sliding with little internal deformation $L > H$ and regions of slow sliding and shearing flow $L < H$. For the situation described above, the ratio of slip length to ice thickness is $L/H = \lambda_N^2/(8\pi^3 AH)$. For a value of A = 0.1 m and a typical ice thickness scale of $H = 1$ km, this suggests that features on scales smaller than $\lambda_N = 150$ m would provide sufficient drag to induce significant vertical shearing within the ice. Since features on this scale are well resolved by the bathymetric profiles (e.g. Figs. 3, 4) and fall within the range of frequencies where the inverse square power law applies, we conclude that the form drag produced by the observed subglacial roughness would have produced significant shearing within the flow of the grounded ice as it retreated over the highs and ridges surveyed by the MBES. This suggests that it is important to include the effects of form drag caused by basal roughness over such terrain, and by extension over the extant parts of TG today.

https://doi.org/10.5194/tc-2020-25
Preprint. Discussion started: 3 February 2020

A distinction must be made for the region of MSGLs on the Dotson-Getz palaeo-ice stream bed (Fig. S1c). Here, the elevation profile is exceptionally smooth. The spectral analysis confirms this (Figs. S4p, q), and the coefficient A that best fits the observations is some two orders of magnitude below the more generally applicable value of A = 0.1 m. Repeating the above analysis with A = 0.001 m shows that the power law would have to apply down to horizontal scales smaller than $\lambda_N = 15$ m. Features on this scale are not well resolved in our bed profiles (e.g. the MBES grids have cell sizes of 50 m). This means that in contrast to the more general case, it remains possible that the MSGL terrain is so smooth that the resulting form drag produces little vertical shearing within the ice that flows over it, making the ice dynamics of this area more akin to the flow described for slippery-based ice streams by MacAyeal (1989). This result is consistent with our understanding of how MSGLs form, i.e. via the self-organisation of deforming sediment at the bed under fast-flowing ice (e.g. Spagnolo et al., 2014). We also repeated the analysis in the direction perpendicular to elongated features (Figs. 7d, S4k-o, q). There is no evidence that ice flowed in this direction, but the theory can nevertheless compute the contributions to form drag that would arise in that hypothetical situation. For most of the across-flow lines (Fig. S4), the power spectra are similar to the along-flow direction, and the drag contributions at each frequency are similar. This suggests that the drag coefficient over much of the surveyed terrain is not especially sensitive to the flow direction.

4 Discussion

4.1 Implications from the new bathymetric and geomorphological data

Our results provide the first observation-based, high-resolution geomorphic characterisation of the coastal bathymetry at TG, a former bed for the glacier. These data allow us to investigate bathymetric controls on ocean circulation towards the modern grounding zone, as well as to identify the locations, water depths and substrate compositions of ice-shelf pinning points and former grounding zones. The dominant bathymetric features, a NNE-SSW trending trough and landward flanking discontinuous ridge (Fig. 2a), represent a subtly different morphologic terrain from highly rugged, basin-dominated areas north and east of the EIS (Fig. 3a) or the moderate-relief areas of lineated terrain with fewer bathymetric highs in eastern Pine Island Bay (Fig. 2a) (Nitsche et al., 2013; Arndt et al., 2018; Kirkham et al., 2019). The continuity and orientation of the trough and ridge relates to the structure of basement rocks on the inner shelf. NNE-SSW to ENE-WSW structural lineaments have been identified by previous aeromagnetic surveys (Gohl, 2012; Gohl et al., 2013), and gravity-derived bathymetries all resolve a broad NNE-SSW ridge coincident with H1-H3, as well as deeper troughs on either side of the ridge (Tinto & Bell, 2011; Millan et al., 2017; Jordan et al., 2020.). Thermochronological analyses of onshore rock samples also infer a NNE-SSW trending tectonic rift structure (Spiegel et al., 2016).

Our results highlight several key differences when compared with the most recent regional bathymetric datasets (Fig. 8). For the area of new MBES data in front of TG, gravity-derived bathymetry generally underestimates sea-floor depths (Figs. 8a, b), whereas the IBCSO bathymetry, which is based on real sea-floor soundings but relies on gravity-inversion elevations and interpolation in this area (Arndt et al., 2013), generally overestimates sea-floor depths (Fig. 8c). All of these datasets fail to

https://doi.org/10.5194/tc-2020-25
Preprint. Discussion started: 3 February 2020


The Cryosphere Discussions

capture the higher-frequency topographic variability revealed by the new MBES data. Although sea-floor highs are sometimes >100 m shallower than the regional products predict, this effect is most notable for the troughs, which are in reality 100 to 550 m deeper than gravity-derived bathymetries, and 50 to 250 m deeper than in the IBCSO dataset (Fig. 8d). When we consider cross-sections of three troughs that are potential pathways for CDW to the grounding zone (T2, T3, T4; locations marked by asterisks in Fig. 8a), the depth errors are up to 500 m, 400 m and 250 m from east to west. Using a conservative top-CDW depth of 500 m for the TG area (based on hydrographic data acquired during NBP19-02; B. Queste, *pers. comm.*; cf. Nakayama et al., 2013), we calculate the cross-sectional area that CDW occupies in these troughs from our MBES data and from the grid of Millan et al. (2017). We find that the gravity-derived bathymetry underestimates the cross-sectional areas by 9%-38% for two of the three troughs, and that trough T2 between H1 and H2 (Fig. 3a) is not resolved at all on the Millan et al. (2017) grid (Table S1; Fig. S5). This discrepancy would lead to a significant underestimation of the volume of CDW that can be transported through the troughs to the ice-shelf cavity and grounding zone of TG (cf. Walker et al., 2007; Arneborg et al., 2012; Table S1), which has implications for ocean circulation modelling of oceanic heat flux, ice-shelf melting, warm-water access to the grounding zone and, ultimately, projected mass loss from TG and the WAIS. The discrepancy underlines the importance of high-resolution observational datasets like MBES for capturing high-amplitude bathymetric variations at short to medium wavelengths (i.e. $\lambda < 10^3$ km), particularly in areas close to ice-shelf cavities and the grounding zone.

Having produced a new gravity-derived bathymetry model for the Thwaites, Crosson and Dotson-Getz area, constrained by the NBP19-02 MBES data, Jordan et al. (*subm.*) similarly determined that high-resolution observations are necessary in areas where knowledge of the bed at scales of less than a few kilometres is required. The need for high-resolution bathymetry was underscored by recent predictive modelling studies of Antarctic outlet glaciers, which conclude that the shape of the ice-shelf cavity and knowledge of small, kilometre-scale pinning points are both key to improving predictions of ice-sheet retreat and sea-level change (Berger et al., 2016; Favier et al., 2016). Similarly, the latest high-resolution ocean models demonstrate that warm deep water reaches the grounding zone of TG through topographically-constrained pathways, again highlighting the critical need for high-resolution bathymetry in making accurate predictions (Nakayama et al., 2019).

The geometry and detailed morphology of the H1-H3 ridge also provide insight on ice-shelf pinning points. Historical grounding-line positions, as mapped from remotely-sensed ice-shelf tidal response, confirm that the Thwaites Ice Shelf is still pinned on high H1 and was pinned on high H2 as recently as 1992 and 2011 (Rignot et al., 2011). By 2011, the area of grounding had reduced to <0.5 km^2 (Fig. 3a) but the recent configuration of the TGT suggests that at least some parts of the TGT remain in (ephemeral) contact with the sea floor. Thus, the exposed H1 and H2 sea-floor highs, and by analogy H3, can be studied as current or recent pinning points for the Thwaites Ice Shelf. Glacial lineations and (or) grounding-zone wedges (GZWs) on the surface of H2 and H3, as well as rare iceberg ploughmarks (Fig. 4b), confirm that these pinning points are mantled by some amount of unconsolidated sediment that can be ploughed or moulded by ice. Sub-bottom profiles over the H2 and H3 highs support this as they show either an incredibly smooth sea-floor response, strongly indicative of unconsolidated sediment cover, or up to 10-15 m of unconsolidated sedimentary units (Fig. S6); furthermore, coring of the top of H3 recovered several meters of sediment (Larter et al., 2020). Although the upper section of the sediment on H3 is glacimarine, deposited

https://doi.org/10.5194/tc-2020-25
Preprint. Discussion started: 3 February 2020

after grounded ice had retreated or lifted-off from the high, the presence of a GZW and on H2 (Figs. 4b, d) suggests that at least the uppermost part of this high may have been constructed via sedimentation at the grounding zone (cf. Alley et al., 1989; 2007). The potential effects of this grounding-zone sedimentation are two-fold: when the TG grounding zone had retreated onto these highs during the Holocene (i.e., at some time after 10.3 cal. ka BP; Hillenbrand et al., 2013), GZW formation could have temporarily slowed further retreat (Alley et al., 2007). Second, continued pinning of an ice shelf on the high and GZW, when most of the grounding line had eventually retreated further landward, would have buttressed the grounded upstream section of TG. The new MBES dataset we present here and the sea floor landforms it reveals, supported by core recovery and sub-bottom profiles, indicate that more sediment is present in this area than is typical of other Amundsen Sea inner shelf environments that experienced rapid ice-sheet retreat, including the adjacent Pine Island Bay and the Dotson-Getz palaeo-ice stream trough (e.g. Larter et al., 2007; Graham et al., 2009; Nitsche et al., 2013, 2016). This is likely because this area immediately offshore TG represents a location where the grounding zone was positioned for a relatively long period of time. Our only constraints on grounding-zone retreat through this area (during the Holocene) are from the core on the H1 high which shows that grounded ice withdrawal from that high by 10.3 cal. ka BP (Hillenbrand et al., 2013) and grounding zones mapped from satellite-era datasets (Rignot et al., 2011). Thus, the TG grounding zone must have been located between H1 and the current grounding zone, potentially on the sea-floor ridges identified here, for thousands of years delivering a significant volume of sediment to the area.

The submarine landforms observed on and around the sea-floor highs raises the question of the composition of these features. Landforms on the flanks of the pinning points (gullies, slide scars, isolated blocks; Fig. 4) may indicate that these highs consist, at least in part, of an erodible material with a probable (hard) bedrock core. In marine settings, slide scars and gullies incise large, pronounced sedimentary scarps like the shelf edge (e.g. Noormets et al., 2009; Gales et al., 2013) or the headwalls of major submarine slides (e.g. Laberg and Vorren, 2000; Vanneste et al., 2006) but do not characterise hard bedrock (crystalline) settings. Further evidence comes from the new observation of planed-off (flat-topped) morphology of the H2 and H3 highs confirming that the upper part of these (down to the level of planing off) consists of a lithology that is erodible by the motion of an ice shelf. Other examples of flat glacial erosion surfaces planed off by ice shelves or flat-based tabular icebergs from the Arctic all document erosion into sedimentary substrates (e.g. Vogt et al., 1994; Jakobsson et al., 2010; Noormets et al., 2016). Small (<100 m high, <5 km wide), flat-topped mounds in the Ross Sea are also thought to consist of unconsolidated volcanogenic deposits rather than crystalline bedrock and, interestingly, GZWs have built up on them, indicating that these features slowed grounding-zone retreat in that area (Lawver et al., 2012; Greenwood et al., 2018). Our interpretation of a proportion of unconsolidated sedimentary substrate, and thus low density material, on the H2 and H3 highs may explain why bathymetries derived from gravity over-estimate the height of some of these features (Figs. 8a, b). In contrast, the morphology of H1 is consistent with it having a crystalline composition, which is supported by the small differences between the water depths of our MBES dataset and the gravity-derived datasets at the H1 location (see proximal 25 km in profile x-x' of Fig. 8d). This very shallow, rugged feature is cross-cut by bedrock grooves and channels typical of hard rock exposures on the inner Antarctic shelf (Lowe and Anderson, 2002; Livingstone et al., 2013) and has no planed-off sections or glacial lineations on its

https://doi.org/10.5194/tc-2020-25
Preprint. Discussion started: 3 February 2020

surface (Fig. 3b). We also note the relative scarcity of bedrock channels or other landforms related to subglacial meltwater flow in the TG MBES dataset with the crescentic scours being the exception. As an example, Kirkham et al. (2019) mapped more than 1000 subglacial channels in Pine Island Bay whereas we map only 175 forms here, albeit over a smaller area. It is not clear whether evidence of previous meltwater routing is buried by sediment in the deep troughs, or has been destroyed by ice flow over the highs. Physical-property and geochemical analyses on cores from the area, acquired as part of *ITGC*, should shed light on the frequency and magnitude of meltwater during the retreat of grounded ice over the sea-floor highs. Schroeder et al. (2013) identified a transition from a distributed channel network with ponded water behind ridges at the modern grounding zone, to a system of concentrated channels downstream. It is possible that a similar configuration for the basal hydrological system occurred as ice retreated over the offshore highs and that evidence is preserved in the marine sedimentary record.

Given the apparent shaping and fragmentation of the H2 and H3 highs (Figs. 4a, b), this observation highlights another potential mechanism influencing glacier dynamics, because if the substrate of a pinning point is soft enough to be moulded by an ice shelf, it might be eroded over time. Erosion of material from the surface of a pinning point, as it is planed off, in conjunction with retrogressive failures at its seaward flank and possibly larger slide or slump events may reduce its height until it cannot serve as a pinning point for the ice shelf (and glacier ice upstream) any longer. This process of unpinning would be exacerbated by increased flow velocities (leading to increased erosion) and/or by ice-shelf thinning, due to either flow acceleration or sub-ice shelf melting, (leading to ungrounding). The result, in a setting with erodible pinning points, is the potential for rapid grounding-zone destabilisation and resulting mass loss, whereby increased ice-flow velocities accelerate pinning point destruction which, in conjunction with simultaneous ice-shelf thinning in response to sub-ice-shelf melting, then promotes ungrounding earlier than would occur on a corresponding “hard”, less erodible pinning point.

4.2 Implications from the new bed roughness data

One major objective of our research is to assess the deglaciated subaqueous terrain offshore from TG as an analogue for the modern bed to gain new insights on TG bed characteristics. The consistency of derived power spectra and drag contributions for bed profiles from the inner ASE shelf and for upstream areas of Pine Island and Thwaites glaciers (Fig. 7) indicates that the roughness properties of the offshore and onshore areas are comparable across all resolvable frequencies. Furthermore, observations confirm that recent grounding-zone retreat affecting TG has occurred over a series of bedrock ridges with the loss of pinning points and formation of new cavities (Tinto & Bell, 2011; Milillo et al., 2019). Further upstream, about 100 km from the recent grounding zone, analyses of radar specularity suggest that the modern TG bed is characterised by high roughness attributed to bedrock cropping out at the glacier base (Schroeder et al., 2014). Our data reveal that the bedrock ridges and intervening troughs underlying the modern grounding zone (Holt et al., 2006; Morlighem et al., 2019), with length scales of tens of kilometres and amplitudes of several hundreds of metres, constitute a morphological terrain similar to the coastal bathymetry (Figs. 2, 3). Further, we demonstrate that this rugged terrain would exert the same strong influence on basal drag for an overriding ice mass (assuming no cavitation) (Figs. 7, SF4). This is consistent with results from inverse methods

https://doi.org/10.5194/tc-2020-25
Preprint. Discussion started: 3 February 2020

to determine basal drag for the modern TG bed, which derive high basal shear stresses near the grounding zone that may explain the steep surface profile of the glacier (Joughin et al., 2009; Arthern et al., 2015). We also note that crag-and-tail landforms (which form subglacially) extend down to the floors of the deep troughs (e.g. Fig. 3, 4b). This confirms that, at least at the time when these features formed, ice of an expanded TG was grounded in the troughs as well as on the highs, and probably experienced high basal shear similar to ice at the present-day grounding zone. The orientation of the crag-and-tails also confirms that ice flow was not directed along troughs but rather overrode the existing topography; this finding is consistent with cosmogenic exposure data from Bear Peninsula (Fig. 1) showing that the ice-sheet surface rose above the top of this terrain during the last glacial period (Johnson et al., 2017).

For shorter wavelengths of bed topography, we can consider the form of the individual sea-floor highs over length scales of several kilometres. We note that these features exhibit the same correlation of morphology with bed type that has been described from on-ice seismic reflection profiles for TG (Muto et al., 2019a, b). Specifically, the correlation is between "hard" beds on the stoss sides of topographic highs, associated with crag-and-tail landforms, and "soft" or sedimentary beds on the lee sides of these features. Although this correlation was based on data from a single along-flow and two across-flow seismic-reflection lines in the upstream area of the glacier, the inference is that this correlation can be applied to the bed in downstream and grounding-zone areas (Muto et al., 2019a, b). This pattern is clearly replicated over the H2 and H3 highs, which have rugged upstream ends with crag-and-tail landforms, glacial lineations over their tops, and sedimentary "tails" on their downstream ends (Fig. 4). This landform pattern is also similar to the 3D morphology of a topographic high near the grounding zone of the Rutford Ice Stream that was imaged using a grid of densely-spaced radar lines (Fig. 4 in King et al., 2016). The correlation of bed types with sea-floor highs (and ridges) holds true for several other areas of the inner shelf around West Antarctica, where streamlining of bedrock highs has often produced landforms with sedimentary tails on the lee sides of bedrock obstacles (e.g. Larter et al., 2009, Graham et al., 2009; Livingstone et al., 2013; Nitsche et al., 2013; 2016), although this is not always the case. Thus, the variability in bed types on topographic highs in offshore regions may provide useful constraints on bed type variability in onshore areas.

Regarding the spectral analysis of roughness and basal drag contributions presented here (Figs. 6, 7, S4), we acknowledge that these only provide an order of magnitude assessment of the contribution to basal drag from the different wavelength scales resolved by the bathymetric DEM (Fig. 2). Analysis beyond the simple 2D-flow line theory used here (see Section 4.2) would be needed to account for 3D-flow effects, and for the nonlinear dependence of ice viscosity on stress (Glen, 1955). Here, we have not been specific about the physical mechanism that controls the smallest roughness wavelength (λ_N). Candidate mechanisms that might limit the influence of roughness at small spatial scales include cavitation (Fowler, 1986), fracture and plucking of crystalline or sedimentary rocks, bulldozing of unconsolidated sediment, or regelation flow around small obstacles (Weertman, 1957). More sophisticated theories accounting for the potential of ice to form cavities in the lee of obstacles could be deployed similarly, but the drag contribution would then depend also on water pressure (Fowler, 1986; Schoof, 2005). Process models of subglacial hydrology, phase change, fracture and sediment transport could all be incorporated in to a more elaborate analysis using MBES datasets as input.

https://doi.org/10.5194/tc-2020-25
Preprint. Discussion started: 3 February 2020

It is clear from our results that the increased spatial resolution of the MBES data is critical for capturing the high-frequency bathymetric variability on the inner continental shelf seaward of TG, which is necessary to understand warm water incursions into sub-ice shelf cavities (Figs. 8, S5; Nakayama et al., 2019). The strong correlation of our observations with interpretations of the present bed conditions of TG and, therefore, the robustness of this deglaciated terrain as an analogue for the modern bed, further demonstrates that more information can be gleaned from this type of marine dataset (i.e. near-continuous bathymetry with spatial resolution better than 0.5 km) For example, the 3D-nature of MBES (with approximately equal resolution in all directions) means that bathymetric variability could be examined in any direction, not only along survey lines, as is the case with onshore radar or seismic-reflection profiles of extant bed topography, and over a variety of spatial scales. These analyses contribute to our understanding of across-flow contributions to basal drag or hydraulic potential (e.g. Muto et al., 2019a), and allow us to constrain the spatial variability of bed types (sediment vs. hard beds, thickness of deformable till, grain size distribution of subglacial sediments), particularly if the sea-floor sediments are cored for ground-truthing. Similarly, the application of theories of subglacial processes as discussed above to high-resolution bathymetric datasets will increase our understanding of ice flow over high-frequency bed roughness, particularly if combined with ultra-high resolution (sub-metre resolution) bathymetries from AUV surveys (e.g. Davies et al., 2017). Indeed, AUV surveys and (or) a dense grid of seismic soundings (only obtainable from non-crevassed ice shelves) are the only way to determine bed geometry in ice-shelf cavities. New techniques such as swath-radar that can image the present glacier bed in 3D, albeit in narrow swaths, have already been trialled on TG (Holschuh et al., 2019) and could be used in conjunction with offshore bathymetric data to build a better-informed, more complete and more uniform resolution picture of basal conditions under TG and at its grounding zone.

5 Conclusion

New 3D bathymetric data from just offshore Thwaites Glacier reveals that the coastal bathymetry is dominated by a ~65 km-long, ~1200 m-deep trough and discontinuous ridge with water depths of 600 m to <100 m. Spatial variations in the morphology of the ridge segments/highs suggest differences in substrate composition along the ridge, with the two southernmost highs having a significant “erodible” component, which is presumably sedimentary in composition. The geometry (flat tops) and landform evidence (glacial lineations, gullies, sediment fans) indicate that the bathymetric highs were planed off and variously eroded by the action of Thwaites Ice Shelf as it flowed over them, presumably reducing the height of these former pinning points over time. A feedback mechanism during unpinning may have occurred, whereby as the ice shelf started to lose contact with the high and frontal buttressing weakened, the resultant increase in flow velocities exacerbated erosion of the high and facilitated further unpinning of Thwaites Glacier.

We present three lines of evidence that this coastal bathymetry provides a good analogue for the modern grounding zone of Thwaites Glacier. First, on length scales of several tens of km the ridge and trough morphology is consistent with the bed topography of the grounding-zone area based on available DEMs and over-ice geophysical data. Second, our spectral decomposition of roughness and basal drag over this rugged, deglaciated terrain is consistent with similar spectral

https://doi.org/10.5194/tc-2020-25
Preprint. Discussion started: 3 February 2020

decompositions, and inversions of basal drag, for profiles from the modern grounding zone area and for areas of the Thwaites bed, where bedrock crops out subglacially (e.g. Schroeder et al., 2014). In contrast, smooth beds, characterised by thick sedimentary substrates and linear glacial landforms, produce distinctly different power spectra and drag contributions. Third, the distribution of landforms and substrate types (unconsolidated sediment vs. bedrock) over the ridge indicates that it displays the same correlation of bed type with topography that has been described for upstream bed areas and inferred for the grounding zone (Muto et al., 2019a, b). As such, further analyses of this deglaciated terrain may provide realistic constraints on across-flow roughness and bed type distribution, and should inform geophysical observations of the modern TG bed that will be acquired as part of *ITGC*.

As discussed above, observational datasets like MBES are required seaward of Antarctic ice shelves in order to capture the high-frequency variability that characterises the bathymetry of nearshore areas. Modelled bathymetry cannot adequately reproduce the km- to sub-km-scale features that are important for accurately calculating inflows of warm ocean water in troughs, and for defining the topographic highs that may act as pinning points for ice shelves and as barriers to warm water incursions.

Author contributions. KAH, RDL, RA, TAJ, AGCG and FON developed the concept of the paper. KAH, RDL, AGCG, RTM, JDK, RC and VF acquired and performed initial processing on the bathymetry data during NBP19-02; JDK performed all channel metric analyses. KG and JEA, and JH provided bathymetric data from German and Korean cruises, respectively. KAH compiled, part-processed and gridded all bathymetric datasets, and wrote the first draft of the paper with substantial contributions from RA and RDL. RA developed the methodology for, performed spectral analyses and basal drag estimations, and wrote the text for these sections; KAH and TAJ provided the profile data. All authors contributed to the development of the final paper and data visualisation.

Competing interests. The authors declare no competing interests.

Acknowledgements. This work is an output of the THwaites Offshore Research (THOR) project and Glacial Habitat of Subglacial Thwaites (GHOST) projects, components of the *International Thwaites Glacier Collaboration* (*ITGC*). Support for this project is from National Science Foundation (NSF: Grant OPP- 1738942) and Natural Environment Research Council (NERC: Grant NE/S006664/1 THOR; Grant NE/S006672/1 GHOST). Logistics were provided by NSF-U.S. Antarctic Program and NERC-British Antarctic Survey. *ITGC* Contribution No. ITGC-011. We thank the NBP19-02 science party, the Edison Chouset Offshore Inc. captain and crew, and the Antarctic Support Contract technical staff aboard the RV/IB *Nathaniel B. Palmer*. This study is part of the Polar Science for Planet Earth Programme of the British Antarctic Survey.

https://doi.org/10.5194/tc-2020-25
Preprint. Discussion started: 3 February 2020

620 **References**

Alley, R. B., Anandakrishnan, S., Dupont, T. K., Parizek, B. R., and Pollard, D.: Effect of sedimentation on ice-sheet grounding-line stability, Science, 315, 1838-1841, 2007.

Alley, R. B., Blankenship, D. D., Rooney, S. T., and Bentley, C. R.: Sedimentation beneath ice shelves -- the view from ice stream B, Marine Geology, 85, 101-120, 1989.

625 Arndt, J. E., Larter, R. D., Friedl, P., Gohl, K., Höppner, K., and the Science Team of Expedition, P. S.: Bathymetric controls on calving processes at Pine Island Glacier, The Cryosphere, 12, 2039-2050, 2018.

Arndt, J. E., Schenke, H. W., Jakobsson, M., Nitsche, F. O., Buys, G., Goleby, B., Rebesco, M., Bohoyo, F., Hong, J., Black, J., Greku, R., Udintsev, G., Barrios, F., Reynoso-Peralta, W., Taisei, M., and Wigley, R.: The International Bathymetric Chart of the Southern Ocean (IBCSO) Version 1.0 – A new bathymetric compilation covering circum-Antarctic waters, Geophysical

630 Research Letters, doi: 10.1002/grl.50413, 2013.

Arneborg, L., Wåhlin, A. K., Björk, G., Liljebladh, B., and Orsi, A. H.: Persistent inflow of warm water onto the central Amundsen shelf, Nature Geoscience, 5, 876-880, 2012.

Arthern, R. J., Hindmarsh, R. C. A., and Williams, C. R.: Flow speed within the Antarctic ice sheet and its controls inferred from satellite observations, Journal of Geophysical Research: Earth Surface, 120, 1171-1188, 2015.

635 Benn, D. I. and J. A. Evans (2010). Glaciers & Glaciation, Hodder Education.

Berger, S., Favier, L., Drews, R., Derwael, J.-J., and Pattyn, F.: The control of an uncharted pinning point on the flow of an Antarctic ice shelf, Journal of Glaciology, 62, 37-45, 2016.

Bingham, R. G., Vaughan, D. G., King, E. C., Davies, D., Cornford, S. L., Smith, A. M., Arthern, R. J., Brisbourne, A. M., De Rydt, J., Graham, A. G. C., Spagnolo, M., Marsh, O. J., and Shean, D. E.: Diverse landscapes beneath Pine Island Glacier

640 influence ice flow, Nature Communications, 8, 1618, 2017.

Caress, D. W. and Chayes, D. N.: Improved processing of Hydrosweep DS multibeam data on the R/V Maurice Ewing, Marine Geophysical Researches, 18, 631-650, 1996.

Caress, D. W., Chayes, D. N., and Ferreira, C.: https://www.mbari.org/products/research-software/mb-system/, last access: 02/12/2019 2019.

645 Cochran, J. R. and Bell, R. E.: IceBridge Sander AIRGrav L1B Geolocated Free Air Gravity Anomalies, V01.5. National Snow and Ice Data Center, Boulder, Colorado, 2010.

Davies, D., Bingham, R. G., Graham, A. G. C., Spagnolo, M., Dutrieux, P., Vaughan, D. G., Jenkins, A., and Nitsche, F. O.: High-resolution sub-ice-shelf seafloor records of twentieth century ungrounding and retreat of Pine Island Glacier, West Antarctica, Journal of Geophysical Research: Earth Surface, 122, 1698-1714, 2017.

650 De Rydt, J. and Gudmundsson, G. H.: Coupled ice shelf-ocean modeling and complex grounding line retreat from a seabed ridge, Journal of Geophysical Research: Earth Surface, 121, 865-880, 2016.

De Rydt, J., Holland, P. R., Dutrieux, P., and Jenkins, A.: Geometric and oceanographic controls on melting beneath Pine Island Glacier, Journal of Geophysical Research: Oceans, 119, 2420–2438, 2014.

Dowdeswell, E. K., Todd, B. J., and Dowdeswell, J. A.: Crag-and-tail features: convergent ice flow through Eclipse Sound, Baffin Island, Arctic Canada, Geological Society, London, Memoirs, 46, 55, 2016.

Dowdeswell, J. A. and Fugelli, E. M. G.: The seismic architecture and geometry of grounding-zone wedges formed at the marine margins of past ice sheets, Geological Society of America Bulletin, 124, 1750-1761, 2012.

Dutrieux, P., Vaughan, D. G., Corr, H. F. J., Jenkins, A., Holland, P. R., Joughin, I., and Fleming, A. H.: Pine Island glacier ice shelf melt distributed at kilometre scales, The Cryosphere, 7, 1543-1555, 2013.

Favier, L., Durand, G., Cornford, S. L., Gudmundsson, G. H., Gagliardini, O., Gillet-Chaulet, F., Zwinger, T., Payne, A. J., and Le Brocq, A. M.: Retreat of Pine Island Glacier controlled by marine ice-sheet instability, Nature Climate Change, 4, 117-121, 2014.

Favier, L., Pattyn, F., Berger, S., and Drews, R.: Dynamic influence of pinning points on marine ice-sheet stability: a numerical study in Dronning Maud Land, East Antarctica, The Cryosphere, 10, 2623-2635, 2016.

Ferrigno, J. G., Lucchitta, B. K., Mullins, K. F., Allison, A. L., Allen, R. J., and Gould, W. G.: Velocity measurements and changes in position of Thwaites Glacier/iceberg tongue from aerial photography, Landsat images and NOAA AVHRR data, Annals of Glaciology, 17, 239-244, 1993.

Fowler, A. C. and Nye, J. F.: A sliding law for glaciers of constant viscosity in the presence of subglacial cavitation, Proceedings of the Royal Society of London. A. Mathematical and Physical Sciences, 407, 147-170, 1986.

Gales, J. A., Larter, R. D., Mitchell, N. C., and Dowdeswell, J. A.: Geomorphic signature of Antarctic submarine gullies: Implications for continental slope processes, Marine Geology, 337, 112-124, 2013.

Glen, J. W. and Perutz, M. F.: The creep of polycrystalline ice, Proceedings of the Royal Society of London. Series A. Mathematical and Physical Sciences, 228, 519-538, 1955.

Gohl, K.: The Expedition of the Research Vessel “Polarstern” to the Amundsen Sea, Antarctica, in 2010 (ANT-XXVI/3), Berichte zur Polar- und Meeresforschung 617, 169 pp, 2010.

Gohl, K.: The Expedition PS104 of the Research Vessel POLARSTERN to the Amundsen Sea in 2017, Berichte zur Polar- und Meeresforschung 712, 100 pp, https://doi.org/10.2312/BzPM_0712_2017, 2017.

Gohl, K.: Basement control on past ice sheet dynamics in the Amundsen Sea Embayment, West Antarctica, Palaeogeography, Palaeoclimatology, Palaeoecology, 335-336, 35-41, 2012.

Gohl, K., Denk, A., Eagles, G., and Wobbe, F.: Deciphering tectonic phases of the Amundsen Sea Embayment shelf, West Antarctica, from a magnetic anomaly grid, Tectonophysics, 585, 113-123, 2013.

Graham, A. G. C. and Hogan, K. A.: Crescentic scours on palaeo-ice stream beds, Geological Society, London, Memoirs, 46, 221, 2016.

https://doi.org/10.5194/tc-2020-25
Preprint. Discussion started: 3 February 2020

Graham, A. G. C., Larter, R. D., Gohl, K., Hillenbrand, C.-D., Smith, J. A., and Kuhn, G.: Bedform signature of a West Antarctic palaeo-ice stream reveals a multi-temporal record of flow and substrate control, Quaternary Science Reviews, 28, 2774-2793, 2009.

Greenwood, S. L., Simkins, L. M., Halberstadt, A. R. W., Prothro, L. O., and Anderson, J. B.: Holocene reconfiguration and readvance of the East Antarctic Ice Sheet, Nature Communications, 9, 3176, 2018.

Ha, H. K., Wåhlin, A. K., Kim, T. W., Lee, S. H., Lee, J. H., Lee, H. J., Hong, C. S., Arneborg, L., Björk, G., and Kalén, O.: Circulation and Modification of Warm Deep Water on the Central Amundsen Shelf, Journal of Physical Oceanography, 44, 1493-1501, 2014.

Heywood, K. J., Biddle, L. C., Boehme, L., Dutrieux, P., Fedak, M., Jenkins, A., Jones, R. W., Kaiser, J., Mallett, H., Garabato, A. C. N., Renfrew, I. A., Stevens, D. P., and Webber, B. G. M.: Between the Devil and the Deep Blue Sea THE ROLE OF THE AMUNDSEN SEA CONTINENTAL SHELF IN EXCHANGES BETWEEN OCEAN AND ICE SHELVES, Oceanography, 29, 118-129, 2016.

Hillenbrand, C.-D., Kuhn, G., Smith, J. A., Gohl, K., Graham, A. G. C., Larter, R. D., Klages, J. P., Downey, R., Moreton, S. G., Forwick, M., and Vaughan, D. G.: Grounding-line retreat of the West Antarctic Ice Sheet from inner Pine Island Bay, Geology, 41, 35-38, 2013.

Hogan, K. A., Dowdeswell, J. A., and Mienert, J.: New insights into slide processes and seafloor geology revealed by side-scan imagery of the massive Hinlopen Slide, Arctic Ocean margin, Geo-Marine Letters, 33, 325-343, 2013.

Holschuh, N., Christianson, K., Paden, J., Alley, R. B., and Anandakrishnan, S.: Linking postglacial landscapes and subglacial processes through swath radar imaging at Thwaites Glacier, West Antarctica, Madison, WI, USA, 12-17 June 2019.

Holt, J. W., Blankenship, D. D., Morse, D. L., Young, D. A., Peters, M. E., Kempf, S. D., Richter, T. G., Vaughan, D. G., and Corr, H. F. J.: New boundary conditions for the West Antarctic Ice Sheet: Subglacial topography of the Thwaites and Smith glacier catchments, Geophys. Res. Lett., 33, L09502, 2006.

Hughes, T. J.: The weak underbelly of the West Antarctic ice sheet, Journal of Glaciology, 27, 518-525, 1981.

Jacobs, S., Giulivi, C., Dutrieux, P., Rignot, E., Nitsche, F., and Mouginot, J.: Getz Ice Shelf melting response to changes in ocean forcing, Journal of Geophysical Research: Oceans, 118, 4152-4168, 2013.

Jacobs, S., Jenkins, A., Hellmer, H., Giulivi, C., Nitsche, F., Huber, B., and Guerrero, R.: THE AMUNDSEN SEA AND THE ANTARCTIC ICE SHEET, Oceanography, 25, 154-163, 2012.

Jacobs, S. S., Hellmer, H. H., and Jenkins, A.: Antarctic Ice Sheet melting in the southeast Pacific, Geophysical Research Letters, 23, 957-960, 1996.

Jakobsson, M., Anderson, J. B., Nitsche, F. O., Gyllencreutz, R., Kirshner, A. E., Kirchner, N., O'Regan, M., Mohammad, R., and Eriksson, B.: Ice sheet retreat dynamics inferred from glacial morphology of the central Pine Island Bay Trough, West Antarctica, Quaternary Science Reviews, 38, 1-10, 2012.

Jakobsson, M., Nilsson, J., O'Regan, M., Backman, J., Löwemark, L., Dowdeswell, J. A., Mayer, L., Polyak, L., Colleoni, F., Anderson, L., Björk, G., Darby, D., Eriksson, B., Hanslik, D., Hell, B., Marcussen, C., Sellén, E., and Wallin, Å.: An Arctic

Ocean ice shelf during MIS 6 constrained by new geophysical and geological data, Quaternary Science Reviews, 29, 3505-3517, 2010.

Jenkins, A., Dutrieux, P., Jacobs, S. S., McPhail, S. D., Perrett, J. R., Webb, A. T., and White, D.: Observations beneath Pine Island Glacier in West Antarctica and implications for its retreat, Nature Geoscience, 3, 468-472, 2010.

Jenkins, A., Dutrieux, P., Jacobs, S., Steig, E. J., Gudmundsson, G. H., Smith, J., and Heywood, K. J.: Decadal Ocean Forcing and Antarctic Ice Sheet Response LESSONS FROM THE AMUNDSEN SEA, Oceanography, 29, 106-117, 2016.

Johnson, J. S., Smith, J. A., Schaefer, J. M., Young, N. E., Goehring, B. M., Hillenbrand, C.-D., Lamp, J. L., Finkel, R. C., and Gohl, K.: The last glaciation of Bear Peninsula, central Amundsen Sea Embayment of Antarctica: Constraints on timing and duration revealed by in situ cosmogenic 14C and 10Be dating, Quaternary Science Reviews, 178, 77-88, 2017.

Jordan, T. A., Porter, D., Tinto, K., Millan, R., Muto, A., Hogan, K., Larter, R. D., Graham, A. G. C., and Paden, J. D.: New gravity-derived bathymetry for the Thwaites, Crosson and Dotson ice shelves revealing two ice shelf populations, The Cryosphere Discuss., 2020, 1-20, 2020.

Joughin, I., Smith, B. E., and Holland, D. M.: Sensitivity of 21st century sea level to ocean-induced thinning of Pine Island Glacier, Antarctica, Geophysical Research Letters, 37, 2010.

Joughin, I., Smith, B. E., and Medley, B.: Marine Ice Sheet Collapse Potentially Under Way for the Thwaites Glacier Basin, West Antarctica, Science, 344, 735, 2014.

Kim, J.-W., Kim, D.-j., Kim, S. H., Ha, H. K., and Lee, S. H.: Disintegration and acceleration of Thwaites Ice Shelf on the Amundsen Sea revealed from remote sensing measurements, GIScience & Remote Sensing, 52, 498-509, 2015.

King, E. C., Pritchard, H. D., and Smith, A. M.: Subglacial landforms beneath Rutford Ice Stream, Antarctica: detailed bed topography from ice-penetrating radar, Earth Syst. Sci. Data, 8, 151-158, 2016.

Kirkham, J. D., Hogan, K. A., Larter, R. D., Arnold, N. S., Nitsche, F. O., Golledge, N. R., and Dowdeswell, J. A.: Past water flow beneath Pine Island and Thwaites glaciers, West Antarctica, The Cryosphere, 13, 1959-1981, 2019.

Kuhn, G., Hillenbrand, C.-D., Kasten, S., Smith, J. A., Nitsche, F. O., Frederichs, T., Wiers, S., Ehrmann, W., Klages, J. P., and Mogollón, J. M.: Evidence for a palaeo-subglacial lake on the Antarctic continental shelf, Nature Communications, 8, 15591, 2017.

Larter, R. D., Graham, A. G. C., Gohl, K., Kuhn, G., Hillenbrand, C.-D., Smith, J. A., Deen, T. J., Livermore, R. A., and Schenke, H.-W.: Subglacial bedforms reveal complex basal regime in a zone of paleo–ice stream convergence, Amundsen Sea embayment, West Antarctica, Geology, 37, 411-414, 2009.

Larter, R. D., Queste, B. Y., Boehme, L., Braddock, S., Wåhlin, A. K., Graham, A. G. C., Hogan, K. A., Totten Minzoni, R., Barham, M., Bortolotto de'Oliveira, G., Clark, R., Fitzgerald, V., Karam, S., Kirkham, J. D., Mazur, A., Sheehan, P., Spoth, M., Stedt, P., Welzenbach, L. Zheng, Y., Andersson, J., Rolandsson, J., Beeler, C., Goodell, J., Rush, and Snow, T.: CRUISE REPORT RV/IB Nathaniel B. Palmer Cruise NBP19-02, January-March 2019: First research cruise of the International Thwaites Glacier Collaboration, 2020.

Larter, R. D. and Vanneste, L. E.: Relict subglacial deltas on the Antarctic Peninsula outer shelf, Geology, 23, 33-36, 1995.

Livingstone, S. J., Cofaigh, C. Ó., Stokes, C. R., Hillenbrand, C.-D., Vieli, A., and Jamieson, S. S. R.: Glacial geomorphology of Marguerite Bay Palaeo-Ice stream, western Antarctic Peninsula, Journal of Maps, 9, 558-572, 2013.

Lowe, A. L. and Anderson, J. B.: Evidence for abundant subglacial meltwater beneath the paleo-ice sheet in Pine Island Bay, Antarctica, Journal of Glaciology, 49, 125-138, 2003.

Lowe, A. L. and Anderson, J. B.: Reconstruction of the West Antarctic ice sheet in Pine Island Bay during the Last Glacial Maximum and its subsequent retreat history, Quaternary Science Reviews, 21, 1879-1897, 2002.

MacAyeal, D. R.: Large-scale ice flow over a viscous basal sediment: Theory and application to ice stream B, Antarctica, Journal of Geophysical Research: Solid Earth, 94, 4071-4087, 1989.

MacLean, B., Blasco, S., Bennett, R., Hughes Clarke, J. E., and Patton, E.: Crag-and-tail features, Amundsen Gulf, Canadian Arctic Archipelago, Geological Society, London, Memoirs, 46, 53, 2016.

MacGregor, J. A., Catania, G. A., Markowski, M. S., and Andrews, A. G.: Widespread rifting and retreat of ice-shelf margins in the eastern Amundsen Sea Embayment between 1972 and 2011, Journal of Glaciology, 58, 458-466, 2012.

Mayer, L. A., Paton, M., Gee, L., Gardner, S. V., and Ware, C.: Interactive 3-D visualization: a tool for seafloor navigation, exploration and engineering, 11-14 Sept. 2000 2000, 913-919 vol.912.

McMillan, M., Shepherd, A., Sundal, A., Briggs, K., Muir, A., Ridout, A., Hogg, A., and Wingham, D.: Increased ice losses from Antarctica detected by CryoSat-2, Geophysical Research Letters, 41, 3899-3905, 2014.

Milillo, P., Rignot, E., Rizzoli, P., Scheuchl, B., Mouginot, J., Bueso-Bello, J., and Prats-Iraola, P.: Heterogeneous retreat and ice melt of Thwaites Glacier, West Antarctica, Science Advances, 5, eaau3433, 2019.

Millan, R., Rignot, E., Bernier, V., Morlighem, M., and Dutrieux, P.: Bathymetry of the Amundsen Sea Embayment sector of West Antarctica from Operation IceBridge gravity and other data, Geophysical Research Letters, 44, 1360-1368, 2017.

Morlighem, M., Rignot, E., Binder, T., Blankenship, D., Drews, R., Eagles, G., Eisen, O., Ferraccioli, F., Forsberg, R., Fretwell, P., Goel, V., Greenbaum, J. S., Gudmundsson, H., Guo, J., Helm, V., Hofstede, C., Howat, I., Humbert, A., Jokat, W., Karlsson, N. B., Lee, W. S., Matsuoka, K., Millan, R., Mouginot, J., Paden, J., Pattyn, F., Roberts, J., Rosier, S., Ruppel, A., Seroussi, H., Smith, E. C., Steinhage, D., Sun, B., Broeke, M. R. v. d., Ommen, T. D. v., Wessem, M. v., and Young, D. A.: Deep glacial troughs and stabilizing ridges unveiled beneath the margins of the Antarctic ice sheet, Nature Geoscience, doi: 10.1038/s41561-019-0510-8, 2019. 2019.

Mouginot, J., Rignot, E., and Scheuchl, B.: Continent-Wide, Interferometric SAR Phase, Mapping of Antarctic Ice Velocity, Geophysical Research Letters, 46, 9710-9718, 2019.

Mouginot, J., Rignot, E., and Scheuchl, B.: Sustained increase in ice discharge from the Amundsen Sea Embayment, West Antarctica, from 1973 to 2013, Geophysical Research Letters, 41, 1576-1584, 2014.

Muto, A., Alley, R. B., Parizek, B. R., and Anandakrishnan, S.: Bed-type variability and till (dis)continuity beneath Thwaites Glacier, West Antarctica, Annals of Glaciology, doi: 10.1017/aog.2019.32. 1-9, 2019a.

Muto, A., Anandakrishnan, S., Alley, R. B., Horgan, H. J., Parizek, B. R., Koellner, S., Christianson, K., and Holschuh, N.: Relating bed character and subglacial morphology using seismic data from Thwaites Glacier, West Antarctica, Earth and Planetary Science Letters, 507, 199-206, 2019b.

Nakayama, Y., Manucharyan, G., Zhang, H., Dutrieux, P., Torres, H. S., Klein, P., Seroussi, H., Schodlok, M., Rignot, E., and Menemenlis, D.: Pathways of ocean heat towards Pine Island and Thwaites grounding lines, Scientific Reports, 9, 16649, 2019.

Nakayama, Y., Schröder, M., and Hellmer, H. H.: From circumpolar deep water to the glacial meltwater plume on the eastern Amundsen Shelf, Deep Sea Research Part I: Oceanographic Research Papers, 77, 50-62, 2013.

Nitsche, F. O., Gohl, K., Larter, R. D., Hillenbrand, C. D., Kuhn, G., Smith, J. A., Jacobs, S., Anderson, J. B., and Jakobsson, M.: Paleo ice flow and subglacial meltwater dynamics in Pine Island Bay, West Antarctica, The Cryosphere, 7, 249-262, 2013.

Nitsche, F. O., Jacobs, S. S., Larter, R. D., and Gohl, K.: Bathymetry of the Amundsen Sea continental shelf: Implications for geology, oceanography, and glaciology, Gechemistry Geophysics Geosystems, 8, Q10009, 2007.

Nitsche, F. O., Larter, R. D., Gohl, K., Graham, A. G. C., and Kuhn, G.: Crag-and-tail features on the Amundsen Sea continental shelf, West Antarctica, Geological Society, London, Memoirs, 46, 199, 2016.

Noormets, R., Dowdeswell, J. A., Larter, R. D., Ó Cofaigh, C., and Evans, J.: Morphology of the upper continental slope in the Bellingshausen and Amundsen Seas - Implications for sedimentary processes at the shelf edge of West Antarctica, Marine Geology, In Press, Corrected Proof, 2009.

Noormets, R., Kirchner, N., Flink, A. E., and Dowdeswell, J. A.: Possible iceberg-produced submarine terraces in Hambergbukta, Spitsbergen, Geological Society, London, Memoirs, 46, 101, 2016.

Parizek, B. R. and Walker, R. T.: Implications of initial conditions and ice–ocean coupling for grounding-line evolution, Earth and Planetary Science Letters, 300, 351-358, 2010.

Pattyn, F. and Van Huele, W.: Power law or power flaw?, Earth Surface Processes and Landforms, 23, 761-767, 1998.

Post, A. L., O'Brien, P. E., Edwards, S., Carroll, A. G., Malakoff, K., and Armand, L. K.: Upper slope processes and seafloor ecosystems on the Sabrina continental slope, East Antarctica, Marine Geology, doi: https://doi.org/10.1016/j.margeo.2019.106091, 2019. 106091, 2019.

Rabus, B. T., Lang, O., and Adolphs, U.: Interannual velocity variations and recent calving of Thwaites Glacier Tongue, West Antarctica, Annals of Glaciology, 36, 215-224, 2003.

Rignot, E.: Evidence for rapid retreat and mass loss of Thwaites Glacier, West Antarctica, Journal of Glaciology, 47, 213-222, 2001.

Rignot, E., Jacobs, S., Mouginot, J., and Scheuchl, B.: Ice-Shelf Melting Around Antarctica, Science, 341, 266-270, 2013.

Rignot, E., Mouginot, J., Morlighem, M., Seroussi, H., and Scheuchl, B.: Widespread, rapid grounding line retreat of Pine Island, Thwaites, Smith, and Kohler glaciers, West Antarctica, from 1992 to 2011, Geophysical Research Letters, 41, 3502-3509, 2014.

https://doi.org/10.5194/tc-2020-25
Preprint. Discussion started: 3 February 2020

Rignot, E., Mouginot, J., and Scheuchl, B.: Antarctic grounding line mapping from differential satellite radar interferometry, Geophysical Research Letters, 38, 2011.

Rignot, E., Mouginot, J., Scheuchl, B., van den Broeke, M., van Wessem, M. J., and Morlighem, M.: Four decades of Antarctic Ice Sheet mass balance from 1979–2017, Proceedings of the National Academy of Sciences, 116, 1095, 2019.

Scambos, T. A., Bell, R. E., Alley, R. B., Anandakrishnan, S., Bromwich, D. H., Brunt, K., Christianson, K., Creyts, T., Das, S. B., DeConto, R., Dutrieux, P., Fricker, H. A., Holland, D., MacGregor, J., Medley, B., Nicolas, J. P., Pollard, D., Siegfried, M. R., Smith, A. M., Steig, E. J., Trusel, L. D., Vaughan, D. G., and Yager, P. L.: How much, how fast?: A science review and outlook for research on the instability of Antarctica's Thwaites Glacier in the 21st century, Global and Planetary Change, 153, 16-34, 2017.

Schoof, C.: Basal perturbations under ice streams: form drag and surface expression, Journal of Glaciology, 48, 407-416, 2002.

Schoof, C.: The effect of cavitation on glacier sliding, Proceedings of the Royal Society A: Mathematical, Physical and Engineering Sciences, 461, 609-627, 2005.

Schoof, C.: Ice sheet grounding line dynamics: Steady states, stability, and hysteresis, Journal of Geophysical Research: Earth Surface, 112, n/a-n/a, 2007.

Schroeder, D. M., Blankenship, D. D., and Young, D. A.: Evidence for a water system transition beneath Thwaites Glacier, West Antarctica, Proceedings of the National Academy of Sciences, 110, 12225, 2013.

Schroeder, D. M., Blankenship, D. D., Young, D. A., Witus, A. E., and Anderson, J. B.: Airborne radar sounding evidence for deformable sediments and outcropping bedrock beneath Thwaites Glacier, West Antarctica, Geophysical Research Letters, 41, 7200-7208, 2014.

Shepherd, A., Gilbert, L., Muir, A. S., Konrad, H., McMillan, M., Slater, T., Briggs, K. H., Sundal, A. V., Hogg, A. E., and Engdahl, M. E.: Trends in Antarctic Ice Sheet Elevation and Mass, Geophysical Research Letters, 46, 8174-8183, 2019.

Spagnolo, M., Clark, C. D., Ely, J. C., Stokes, C. R., Anderson, J. B., Andreassen, K., Graham, A. G. C., and King, E. C.: Size, shape and spatial arrangement of mega-scale glacial lineations from a large and diverse dataset, Earth Surface Processes and Landforms, 39, 1432-1448, 2014.

Spiegel, C., Lindow, J., Kamp, P. J. J., Meisel, O., Mukasa, S., Lisker, F., Kuhn, G., and Gohl, K.: Tectonomorphic evolution of Marie Byrd Land – Implications for Cenozoic rifting activity and onset of West Antarctic glaciation, Global and Planetary Change, 145, 98-115, 2016.

Tinto, K. J. and Bell, R. E.: Progressive unpinning of Thwaites Glacier from newly identified offshore ridge: Constraints from aerogravity, Geophysical Research Letters, 38, 2011.

Vanneste, M., Mienert, J., and Bünz, S.: The Hinlopen Slide: A giant, submarine slope failure on the northern Svalbard margin, Arctic Ocean, Earth and Planetary Science Letters, 245, 373-388, 2006.

Vaughan, D. G. and Arthern, R.: Why Is It Hard to Predict the Future of Ice Sheets?, Science, 315, 1503, 2007.

https://doi.org/10.5194/tc-2020-25
Preprint. Discussion started: 3 February 2020

Vaughan, D. G., Corr, H. F. J., Ferraccioli, F., Frearson, N., O'Hare, A., Mach, D., Holt, J. W., Blankenship, D. D., Morse, D. L., and Young, D. A.: New boundary conditions for the West Antarctic ice sheet: Subglacial topography beneath Pine Island Glacier, Geophys. Res. Lett., 33, L09501, 2006.

Vogt, P. R., Crane, K., and Sundvor, E.: Deep Pleistocene iceberg plowmarks on the Yermak Plateau: sidescan and 3.5 kHz evidence for thick calving ice fronts and a possible marine ice sheet in the Arctic Ocean, Geology, 22, 403-406, 1994.

Walker, D. P., Brandon, M. A., Jenkins, A., Allen, J. T., Dowdeswell, J. A., and Evans, J.: Oceanic heat transport onto the Amundsen Sea shelf through a submarine glacial trough, Geophysical Research Letters, 34, 2007.

Weertman, J.: On the Sliding of Glaciers, Journal of Glaciology, 3, 33-38, 1957.

Weertman, J.: Stability of the junction between an ice sheet and an ice shelf, Journal of Glaciology, 13, 3-11, 1974.

Welch, P. D.: The Use of Fast Fourier Transform for the Estimation of Power Spectra: A Method Based on Time Averaging Over Short, Modified Periodograms, IEEE TRANSACTIONS ON AUDIO AND ELECTROACOUSTICS, 15, 70-73, 1967.

Wellner, J. S., Heroy, D. C., and Anderson, J. B.: The death mask of the Antarctic ice sheet: Comparison of glacial geomorphic features across the continental shelf, Geomorphology, 75, 157-171, 2006.

Yu, H., Rignot, E., Seroussi, H., Morlighem, M., and Choi, Y.: Impact of Iceberg Calving on the Retreat of Thwaites Glacier, West Antarctica Over the Next Century With Different Calving Laws and Ocean Thermal Forcing, Geophysical Research Letters, 46, https://doi.org/10.1029/2019GL084066, 2019.

https://doi.org/10.5194/tc-2020-25
Preprint. Discussion started: 3 February 2020

Cruise ID	**Year**	**Multibeam echo sounder (frequency)**	**Source** Data centre and *lead institution*
NBP19-02	2019	Kongsberg EM122 (12 kHz)	IEDA MGDS *BAS/Univ. Houston*
NBP19-01	2019	Kongsberg EM122 (12 kHz)	IEDA MGDS *Stanford/Caltech*
PS104	2017	Hydrosweep DS-2 (15.5 kHz)	*AWI*
JR294	2014	Kongsberg EM122 (12 kHz)	UK PDC *Univ. East Anglia*
ANT-XXVI/3	2010	Hydrosweep DS-2 (15.5 kHz)	*AWI*
NBP09-01	2009	Kongsberg EM120 (12 kHz)	IEDA MGDS *LDEO*
JR179	2008	Kongsberg EM120 (12 kHz)	UK PDC *BAS*
NBP07-02	2007	Kongsberg EM120 (12 kHz)	IEDA MGDS *LDEO*
JR141	2006	Kongsberg EM120 (12 kHz)	UK PDC *BAS*
NBP00-01	2000	SeaBeam 2112 (12 kHz)	IEDA MGDS *Rice University*
NBP99-02	1999	SeaBeam 2112 (12 kHz)	IEDA MGDS *Rice University*
ANA02C	2012	Kongsberg EM122 (12 kHz)	KOPRI

Table 1: Research cruises that acquired MBES data used in this compilation. IEDA MGDS is the Interdisciplinary Earth Data Alliance Marine Geoscience Data System (USA; http://www.marine-geo.org/index.php); UK PDC is the United Kingdom Polar Data Centre (UK; https://www.bas.ac.uk/data/uk-pdc/); BAS is British Antarctic Survey; AWI is the Alfred Wegener Institute (Germany); LDEO is Lamont-Doherty Earth Observatory of Columbia University; KOPRI is the Korea Polar Research Institute.

https://doi.org/10.5194/tc-2020-25
Preprint. Discussion started: 3 February 2020

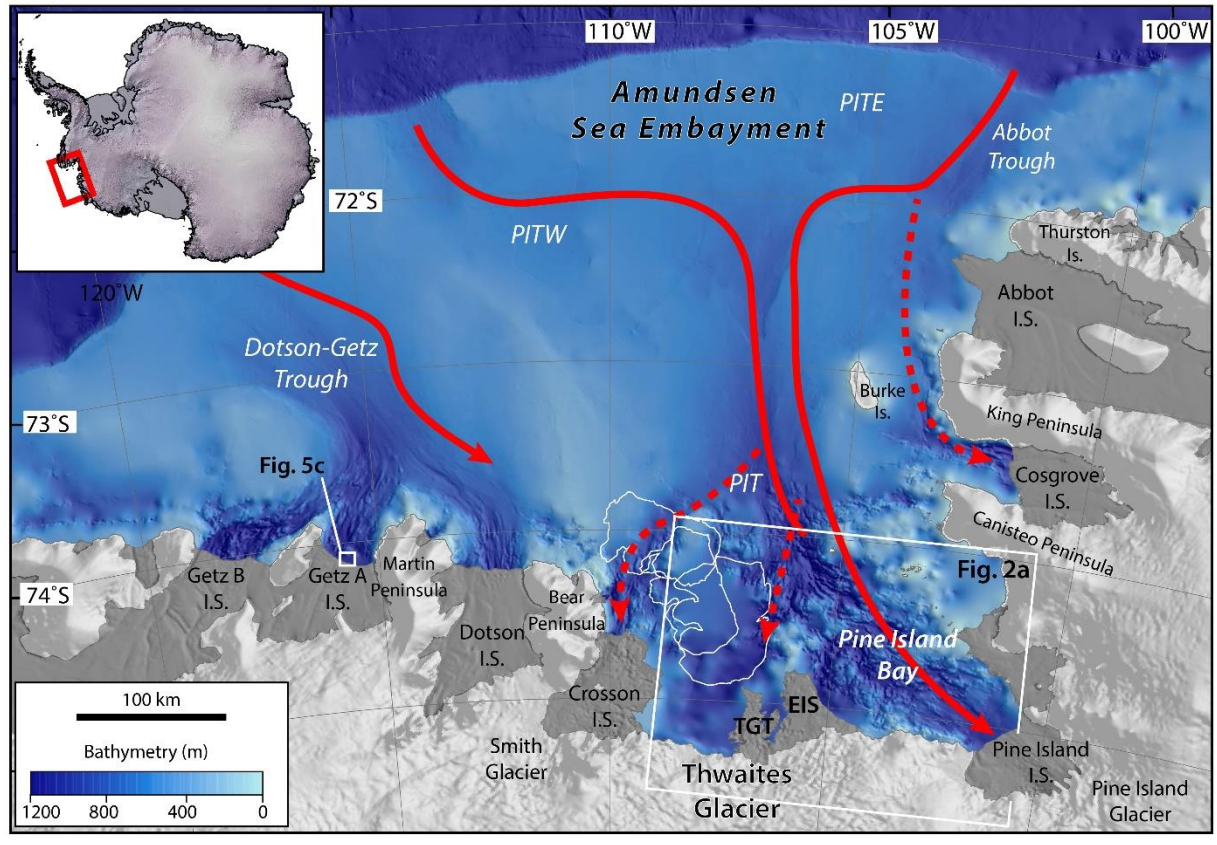

Figure 1: Regional bathymetry for the Amundsen Sea Embayment and location of Thwaites Glacier (TG), West Antarctica. Bathymetry is from IBCSO (Arndt et al., 2013); arrows show observed (solid) and inferred (dashed) pathways for CDW across the continental shelf towards the grounding lines of Pine Island, Thwaites and Smith glaciers (after Nakayama et al., 2013; Dutrieux et al., 2014; Ha et al., 2014 for Dotson-Getz trough). PIT is Pine Island Trough; PITE is Pine Island Trough East; PITW is Pine Island Trough West; TGT is Thwaites Glacier Tongue; EIS is Eastern Ice Shelf; other ice shelves (I.S.) are also labelled. White outlines north of TG are mapped positions of the B-22A iceberg from 2002, 2010 and 2018, from south to north. Note the more "blurry" look of the bathymetry in front of TG (in IBCSO this bathymetry is based on the Tinto & Bell (2011) gravity-inversion and interpolation), where ship access has been hampered before austral summer 2018/2019 by persistent fast ice and the presence of the B-22A iceberg.

https://doi.org/10.5194/tc-2020-25
Preprint. Discussion started: 3 February 2020

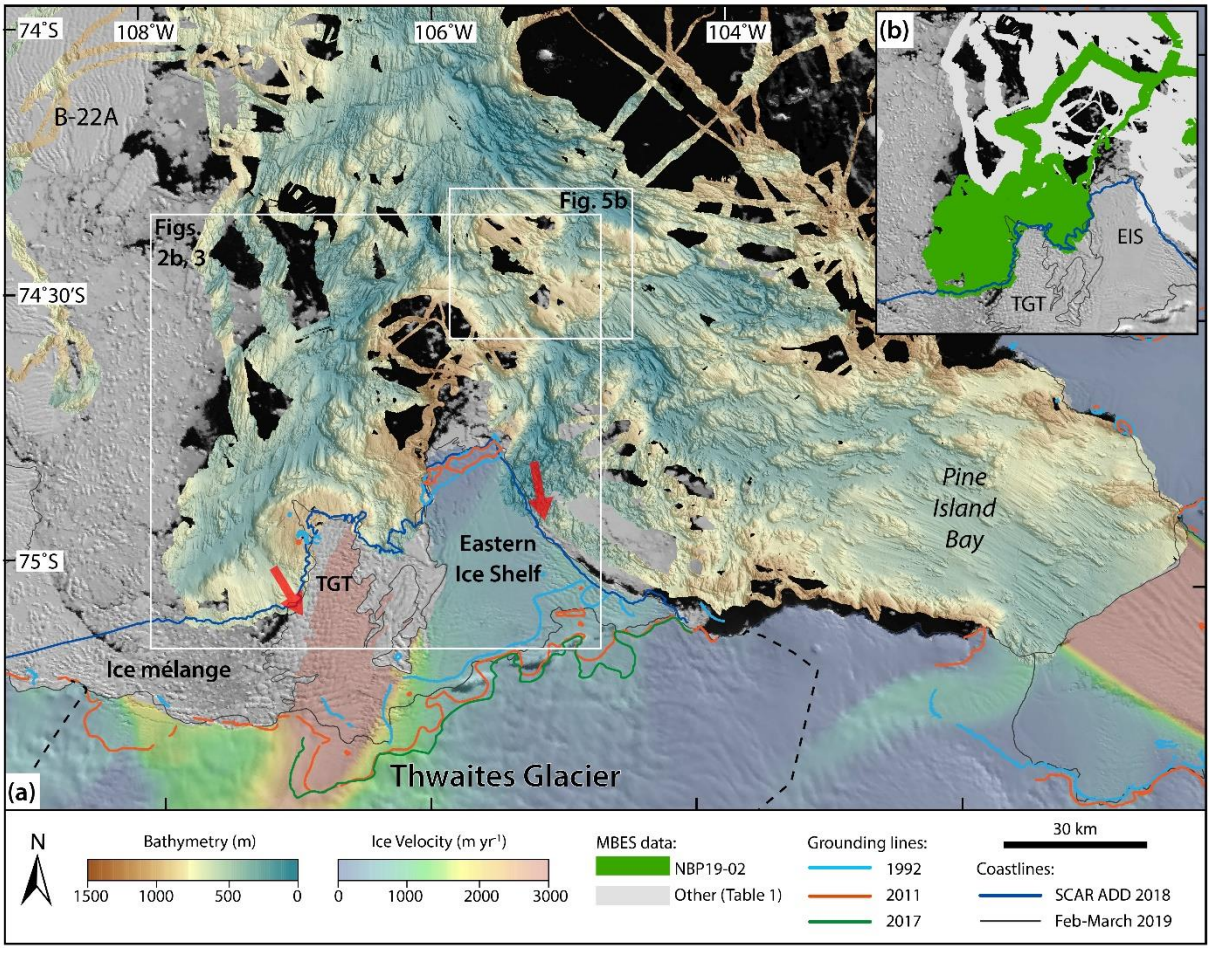

Figure 2: (a) New MBES grid for the inner Amundsen Sea Embayment. Ice-velocity data from the MEaSUREs V2 dataset (Mouginot et al., 2019); grounding lines for 1992 and 2011 are from Rignot et al. (2011), and that for 2017 from Milillo et al. (2019); red arrows 885 **delineate CDW pathways after Dutrieux et al. (2014) and Milillo et al. (2019). The black dashed line marks the boundaries of the drainage basin of Thwaites Glacier (Vaughan et al., 2001). (b) NBP19-02 data coverage versus other MBES datasets (Table 1). The dark blue coastline illustrates the ice-shelf and ice-mélange extent during survey on NBP19-02 and was digitised from Landsat 8 imagery.**

https://doi.org/10.5194/tc-2020-25
Preprint. Discussion started: 3 February 2020

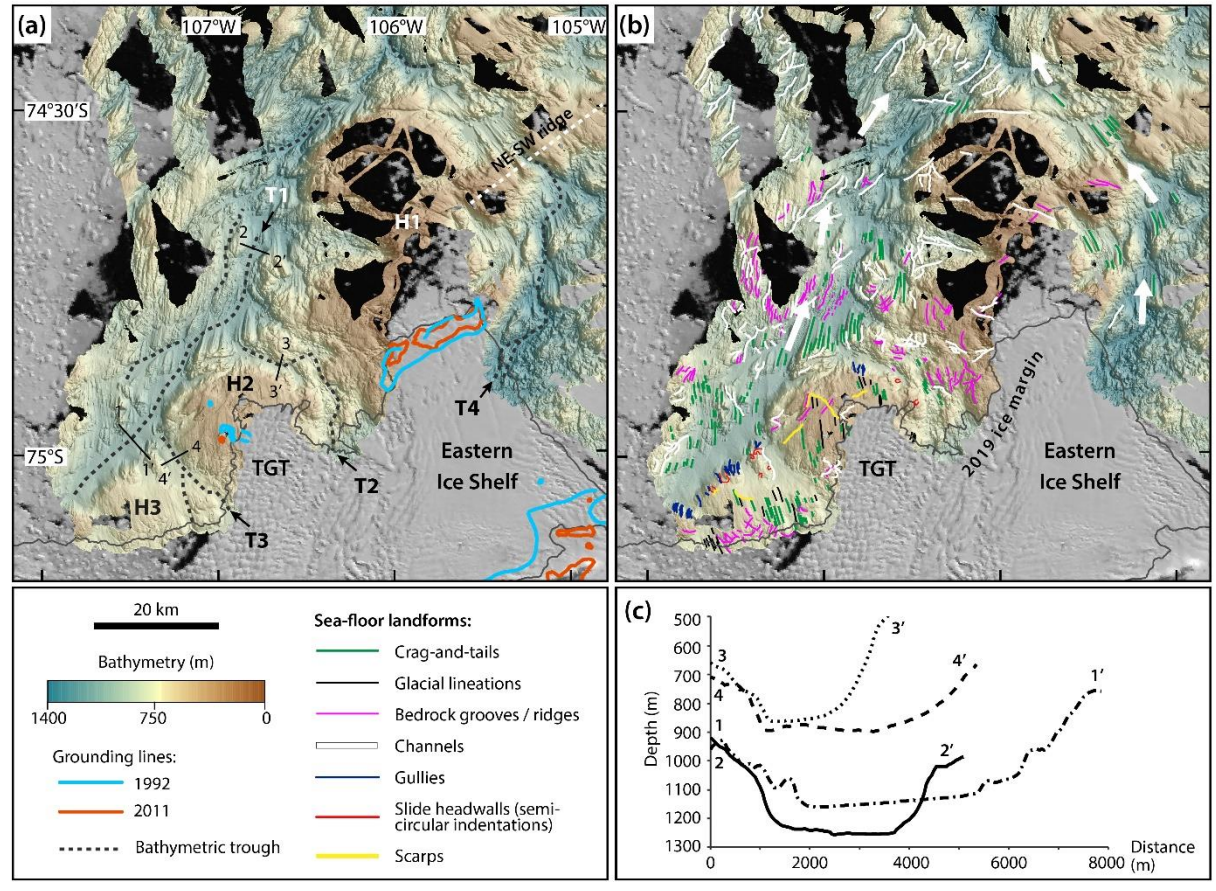

890 **Figure 3:(a) High-resolution bathymetry map of the inner Amundsen Sea shelf in front of TG and the eastern part of Pine Island Bay showing the large-scale sea-floor morphology including bathymetric troughs (T1-T3; main axes highlighted by black dashed lines) and highs (H1-H3) that form a broad NNE-SSW ridge continuing into a ridge further offshore in Pine Island Bay, northeast of the Eastern Ice Shelf (white dashed line). (b) Mapped sea-floor landforms; streamlined features show the former flow direction of an expanded TG (white arrows). (c) Cross-sectional profiles of the bathymetric troughs; locations of profiles in (a).**

895

https://doi.org/10.5194/tc-2020-25
Preprint. Discussion started: 3 February 2020

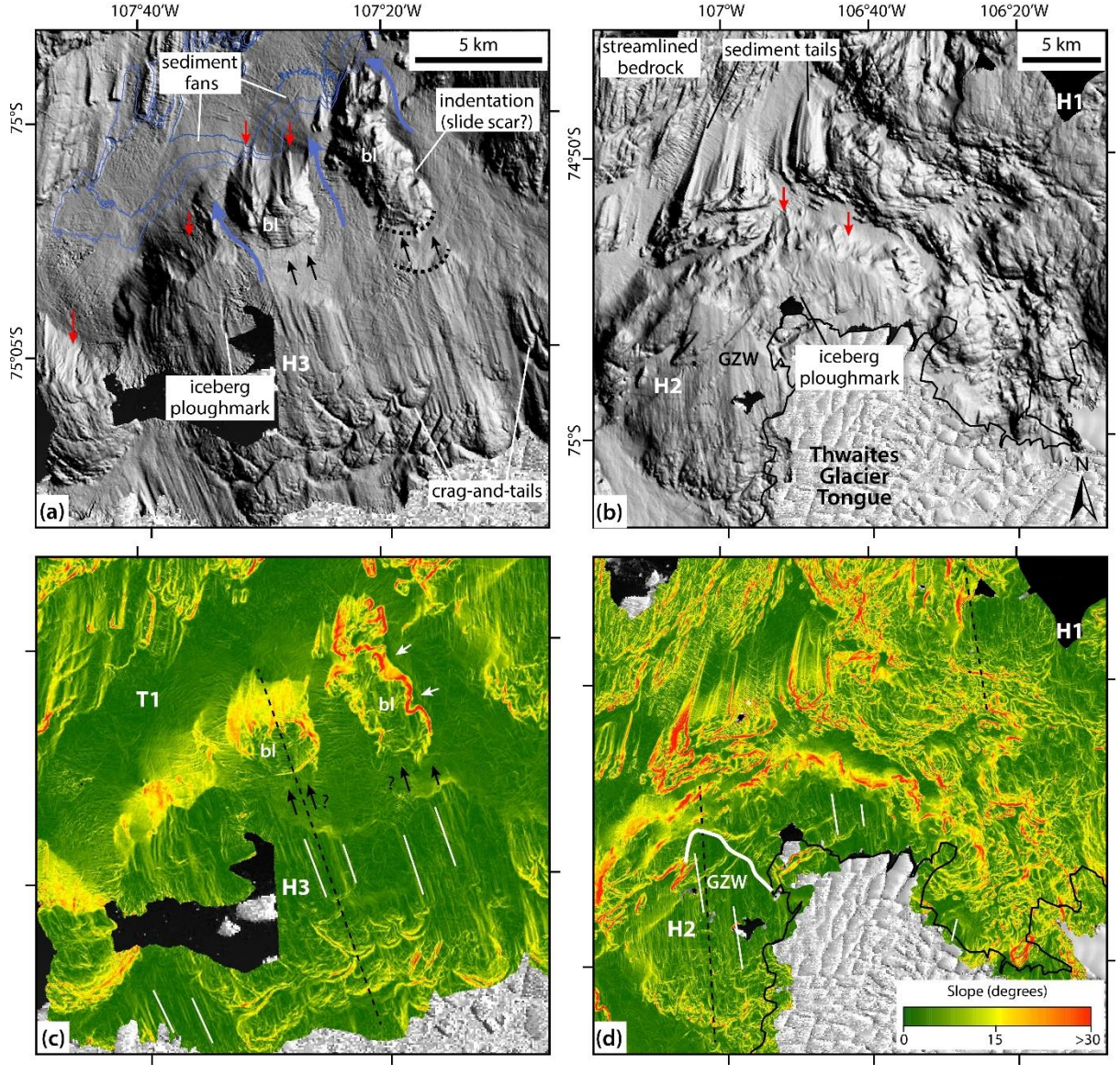

Figure 4: Detailed maps of the MBES data and its first derivative, slope, over the sea-floor highs in front of Thwaites Glacier. (a) and (c) the H3 high. (b) and (d) the H2 high and western flank of H1. Red arrows in (a) and (b) point to gullies incised into the seaward flanks of the highs; the white lines in (c) and (d) mark glacial lineations; bl are the isolated blocks of H3 and black arrows in (a) and (c) denote their possible transport paths), with the black dotted lines in (a) illustrating semi-circular indentations; white arrows in (c) point to a channel at the base of one of the blocks; blue arrows in (a) indicate the down-slope transport direction of material into sediment fans at the front of H3 highlighted by bulges in the contours (contour levels 1100, 1125 and 1150 m). Black dashed lines in (c) and (d) locate the profiles in Fig. 5a. GZW is grounding-zone wedge.

https://doi.org/10.5194/tc-2020-25
Preprint. Discussion started: 3 February 2020

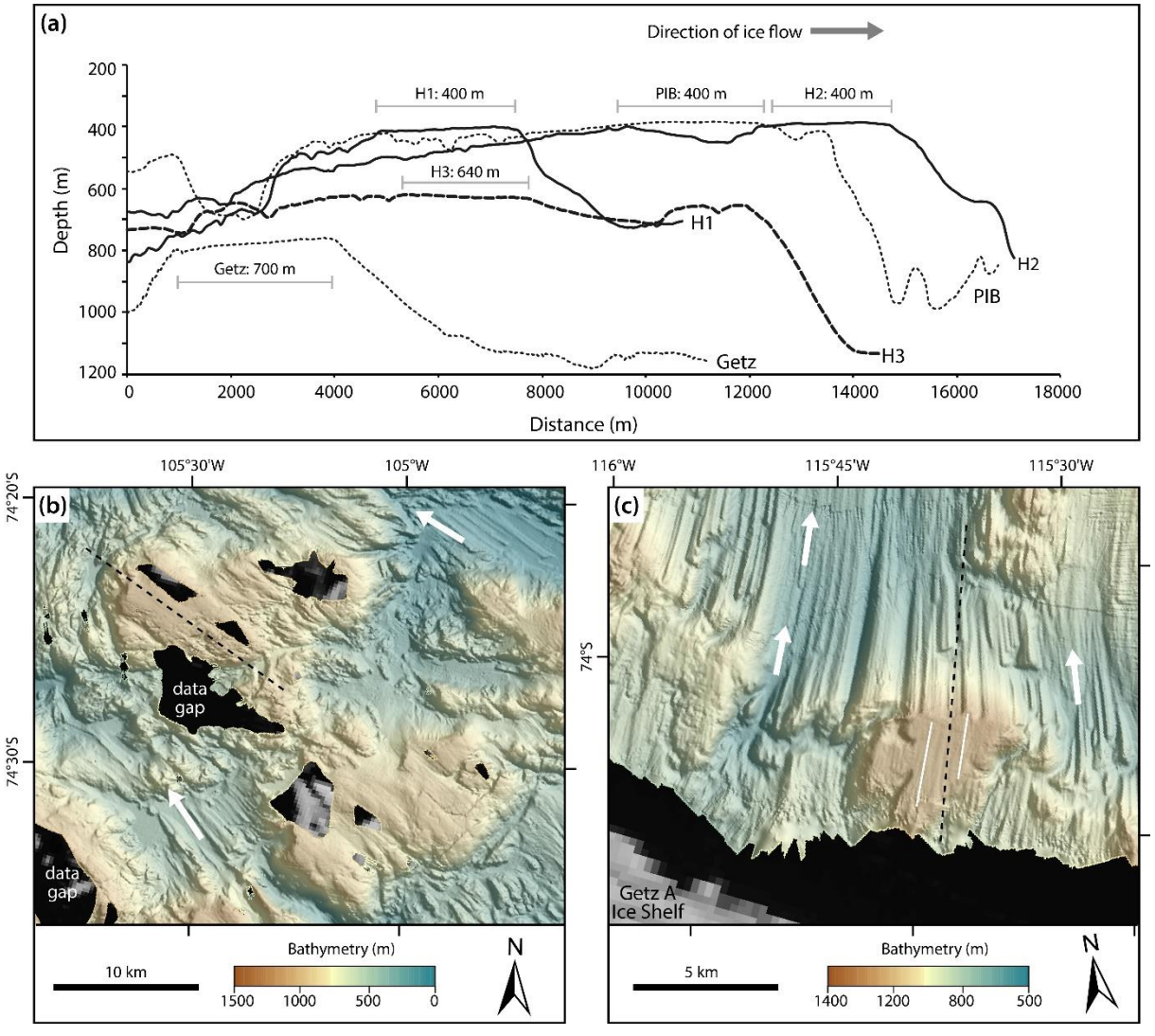

Figure 5: Flat-topped highs in the Amundsen Sea. (a) Cross-sectional profiles over H1-H3 highs at Thwaites Glacier (for location of profiles see Figs. 4c, d), further offshore in Pine Island Bay (PIB; location of high in Fig. 2a, location of profile in Fig. 5b) and offshore from the Getz-A Ice Shelf (location of high in Fig. 1, location of profile in Fig. 5c), showing sea-floor highs planed off at different depth levels. The flat portions of the profiles are marked with grey bars and the depth elevation for that flat-top given above, so "H1:400 m" means the flat part of the profile over H1 high is at 400 m water depth. (b) MBES of flat-topped highs part of the discontinuous sea-floor ridge in PIB. (c) MBES of a flat-topped high with glacial lineations (white lines) just in front of the Getz-A Ice Shelf (after Nitsche et al., 2016). White arrows show direction of past ice flow based on streamlined subglacial landforms.

https://doi.org/10.5194/tc-2020-25
Preprint. Discussion started: 3 February 2020

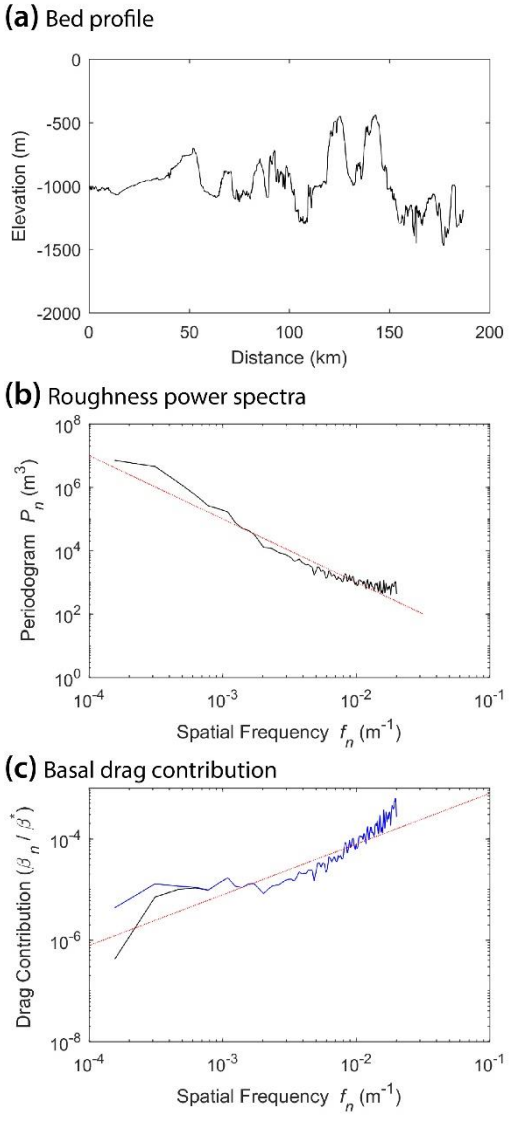

915 **Figure 6: (a) Bed elevation (= water depth for sea-floor data) verses distance along flow line. (b) Roughness power spectra P_n verses spatial frequency f_n. (c) Scaled basal drag contributions β_n/β^* verses f_n for along-flow profile (6) offshore from Pine Island and Thwaites glaciers (for location see Fig. S1a). The red lines in (b) and (c) are based on an assumption of Brown-noise, with variance of roughness decaying as the inverse square of spatial frequency. At low spatial frequencies, drag contributions depend on the function F (see Section 4.2) with the two limiting cases shown: F_1 (blue), F_2 (black).**

920

https://doi.org/10.5194/tc-2020-25
Preprint. Discussion started: 3 February 2020

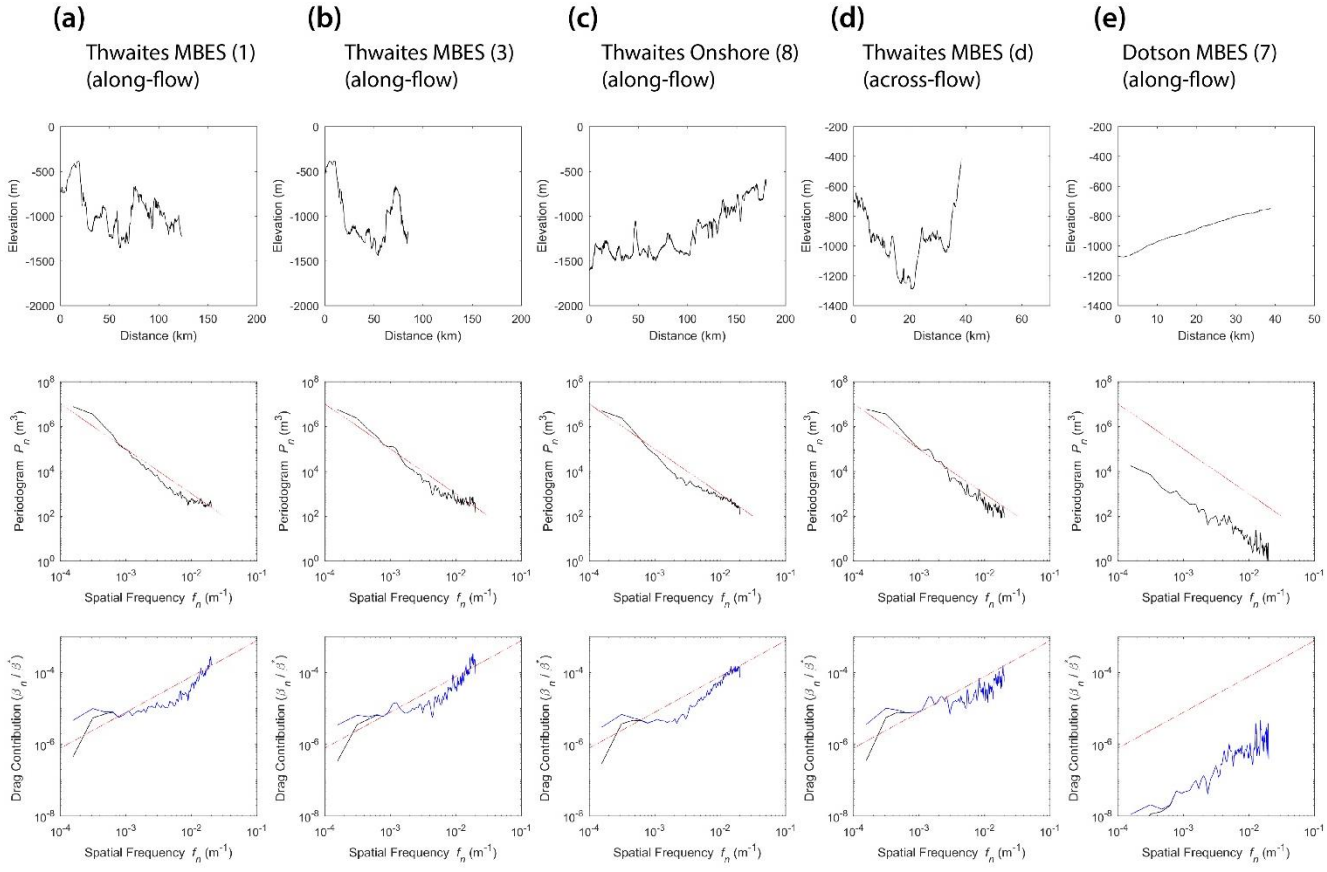

Figure 7: Selection of bed profiles (top), derived power spectra (middle) and basal drag contributions (bottom) for: (a, b) along-flow profiles (1) and (3) offshore Thwaites Glacier; (c) onshore along-flow bed profile (8) for Thwaites Glacier; (d) across-flow profile "d" for offshore TG; (e) along-flow profile (7) for Dotson-Getz Trough. Profile locations are shown in Figs. SF1, SF2. The red line in power spectra and drag contribution plots are based on an assumption of Brownian motion (i.e. power decays as inverse square of spatial frequency). At low spatial frequency, drag contributions depend on the function F. Two limiting cases are shown: F_1 (blue), F_2 (black).

https://doi.org/10.5194/tc-2020-25
Preprint. Discussion started: 3 February 2020

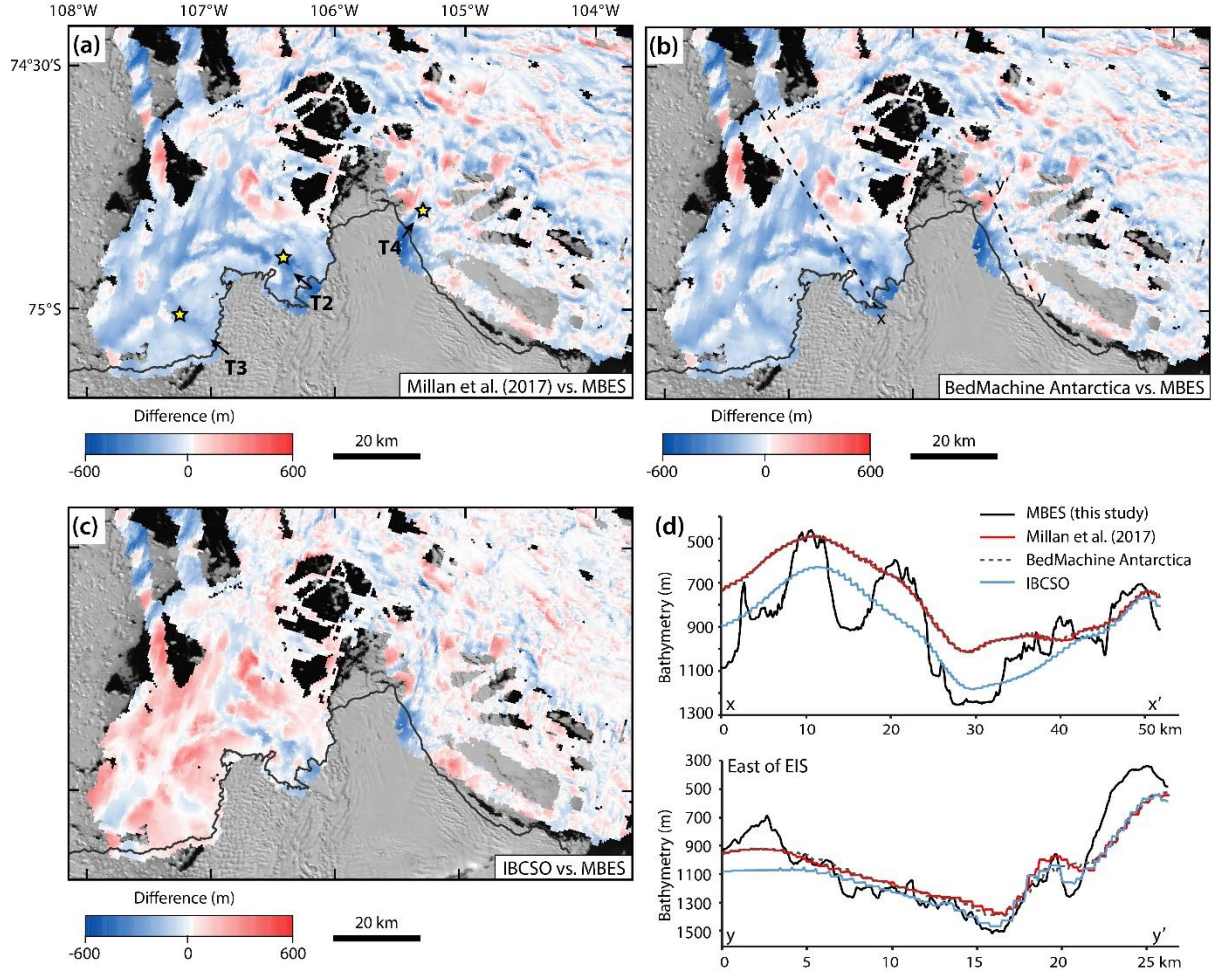

Figure 8: Difference maps between regional bathymetric datasets and the MBES grid. (a) Millan et al. (2017) minus MBES grid. Yellow asterisks mark the locations of channels discussed in Section 5. (b) BedMachine Antarctica (Morlighem et al., 2019) minus MBES grid. (c) IBCSO (Arndt et al., 2013) minus MBES grid. (d) Profile data for two profiles for each of the regional datasets compared with profiles from the MBES grid; profiles are located in (b). Note that the Millan et al. (2017) and the BedMachine Antarctica bathymetries are very similar and thus return near identical bed profiles in (d); the BedMachine Antarctica grid is included for completeness as the most recent regional dataset to cover the area and its authors highlight the need for more coastal bathymetric datasets (Morlighem et al., 2019).